Structures 52 (2023) 506–523

Contents lists available at ScienceDirect

Structures

journal homepage: www.elsevier.com/locate/structures

Probabilistic-based discrete model for the seismic fragility assessment of masonry structures

Luis C.M. da Silva [a,*], Gabriele Milani [a], Paulo B. Lourenço [b]

[a] Department A.B.C., Politecnico di Milano, Piazza Leonardo da Vinci, 20133, Milan, Italy
[b] Department of Civil Engineering, ISISE, University of Minho, Azurém, 4800-058, Guimarães, Portugal

ARTICLE INFO

Keywords:
Masonry
Homogenization
Macro-element
Micro-modelling
Fragility curves
Latin hypercube sampling

ABSTRACT

Classical Finite-Element and Discrete-Element strategies are expensive to carry when analysing masonry structures in the inelastic range, under a seismic excitation, and considering uncertainty. Their application to the seismic fragility assessment of masonry structures through non-linear time-history analysis becomes thus a challenge. The paper addresses such difficulty by presenting an alternative probabilistic-based numerical strategy. The strategy couples a discrete macro-element model at a structural-scale with a homogenization model at a meso-scale. A probabilistic nature is guaranteed through a forward propagation of uncertainty through loading, material, mechanical, and geometrical parameters. An incremental dynamic analysis is adopted, in which several assumptions decrease the required computational time-costs. A random mechanical response of masonry is provided by numerical homogenization, using Latin hypercube sampling with a non-identity correlation matrix, and only a reduced number of representative random samples are transferred to the macro-scale. The approach was applied to the seismic fragility assessment of an English-bond masonry mock-up. Its effectiveness was demonstrated, and its computational attractiveness highlighted. Results may foster its use within the seismic fragility assessment of larger structures, and the opportunity to better analyze the effect of material and geometric-based uncertainties in the stochastic dynamic response of masonry structures.

1. Introduction

Natural disasters that occurred between 2000–2019 affected four billion people and led to 3 trillion U.S. dollars in economic losses [1]. Unpredictable recurrence times of such extreme events urge actions and the United Nations [2] has, through the Sendai Framework 2015–2030, highlighted the importance of scientific research and technology in decision making for disaster risk reduction. This paper aims to contribute to such challenge and addresses both the seismic scenario and masonry structures. Reasons supporting the scope of the work are threefold: (1) earthquakes represent ≈10% of the costs of natural disasters, but are responsible for ≈60% of total fatalities [1]; (2) masonry structures are rather vulnerable to out-of-plane loads [3–11]; and (3) seismic fragility curves are critical for decision-making [12]. Moreover, we intend to contribute with a probabilistic-based model for the seismic assessment of existing masonry structures.

From a deterministic standpoint, several strategies can be found for the structural analysis of masonry structures. At a territorial scale, empirical strategies are generally employed since require limited information [13–16], being also coupled with equivalent-frame methods or other fast and mechanistic-based model to form the so-called hybrid approaches [17–19]. Nevertheless, at a building scale it seems clear that research leans towards the (i) analytical and (ii) numerical approaches [20–23]. Analytical approaches are often based on the theorems of limit analysis and through a force- or displacement-based formulation [24–26]. These are suitable for a rapid seismic fragility assessment [27], but are unable to track the displacements history and damage evolution. To what concerns numerical approaches, the Finite Element Method (FEM) [23,28,29] and the Discrete Element Method (DEM) [30–34] are largely used. DEM is now well suited for masonries with both dry- and mortared joints, but still requires a full representation of the blocks (masonry units) arrangement [31]. FEM allows instead a more versatile application since masonry can be represented either through a continuous equivalent media (designated macro-modelling) or by a discrete representation of units and joints (designated micro-modelling). Linear and non-linear static and dynamic analyses are eligible, but the analysis can be both time-consuming and computationally expensive when estimating the ultimate ductility level of the structure.

To cope with the prohibitive computational cost, multi-scale FE methods seem a promising alternative and are in between the micro-

* Corresponding author.
E-mail address: luiscarlos.martinsdasilva@polimi.it (L.C.M. da Silva).

https://doi.org/10.1016/j.istruc.2023.04.015
Received 6 January 2023; Received in revised form 27 March 2023; Accepted 3 April 2023
Available online 10 April 2023

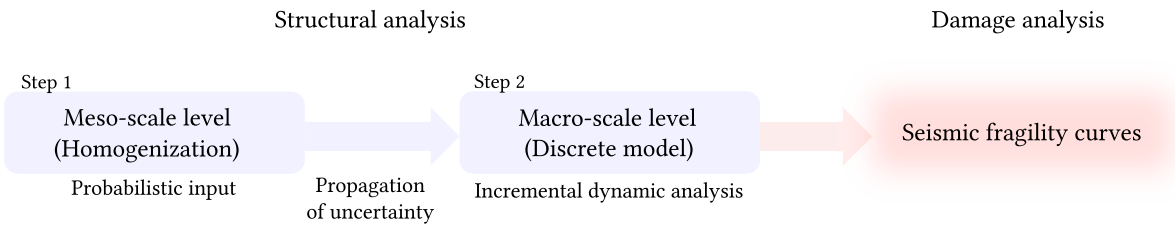

Fig. 1. General framework and steps processed with the probabilistic two-scale numerical strategy.

and macro- FE schemes. Classical FE^2 approaches, based on a full continuum description of the media, seem to have only advantages if a linear elastic behaviour is assumed [35–37] and are thus seldom used for dynamic purposes and complex structural analysis [36]. The development of techniques that keep accuracy to acceptable levels and speed up the processing running times is critical. For instance, the use of discrete FE-based methods is being adopted at a macro-level [5,37]. Two-step approaches with a discrete representation of the media are very practical due to the decrease of the number of degrees of freedom (comparing to a continuous approach) and are useful for dynamic analysis. Several studies have shown the clear advantages of this process since it allows a good trade-off between consumed time and results' accuracy and enables the study of real scale buildings. The latter is even more clear if simplifications are further assumed at both macro- or micro-scales, as observed in [38–44]. Nonetheless, existing masonry structures gather significant uncertainties [45] and the such strategies must be coupled with a probabilistic-based assessment that may offer more confidence to practitioners. Site inspection and experimentation are paramount in lessening such uncertainty, as they provide valuable insight into structure's geometry, boundary conditions, and materials [46,47]. Current standards [48,49] allow evaluating structures according to desired seismic performance levels. Practicability is ensured by adopting a semi probabilistic approach through safety factors calibrated to meet reliability requirements. Final safety verification is yet deterministic – ratio between capacity and demand –, hence may be inadequate when loading uncertainty is high, as witnessed in Japan [50].

Code-alternatives are being recommended and especially within a performance-based methodology (PEER), which seems widely accepted as the state-of-art risk assessment approach [12,51,52]. The PEER methodology tried to introduce uncertainty within all the four stages of a seismic loss assessment study, i.e.: (i) hazard analysis (seismic action); (ii) structural analysis; (iii) damage analysis; and (iv) decision analysis (consequences). Such a framework can be applied for both new and existing structures and at a structural or territorial level. In any case, this appears to be a key tool in the decision process, as it can indicate the best design or retrofit solutions – for new or existing structures, respectively –, to face a future seismic event considering both economic and downtime costs established by the owner and designer [12]. The failure probability of random systems can be found by solving the limit state function integral. Asymptotic methods (FORM/SORM/FOROS/SOROS) [53] are popular due to their simplicity and computational efficiency, but are still hardly used within nonlinear problems. Approximate strategies, such as the response surface method [53,54], surrogate models [53], and sampling methods as the Monte Carlo (MC) or the Latin Hypercube (LH) [45,55] are the most used under multivariate random systems. Sampling methods are generally adopted for both nonlinear and large-scale problems but are rarely combined with nonlinear time-history analysis (NLTHA). From literature, one concludes that performing nonlinear dynamic analysis within full-probabilistic domain is still challenging for masonry structures. Nonlinear dynamics is restricted to simplified modelling strategies, such as SDOF systems [56], frame-based models [45], simplified macro-element and Discrete-Element modelling (DEM) [55,57–60], but a sound work on continuous Finite-Element (FE) strategies is still lacking. Instead, quasi-static analysis is widely assumed [61] regardless of the modelling assumption, with the setback of neglecting important dynamic effects. It appears that further studies on probabilistic assessment of masonry structures are needed. The limited knowledge provided by the JCSS [62] somehow indicates this need.

Under this scope, the study aims filling the existing gap between practical applicability of classical FE/DEM strategies and the need of modelling masonry with accurate approaches in the inelastic range, under dynamic loads, and considering uncertainty. The latter is achieved by presenting a probabilistic numerical strategy based on a two-scale (FE^2) approach, in which a discrete FE-based macro-element model at a structural level is coupled with a homogenization FE model at a meso-scale. A LH sampling technique, for which all system variables can be random, allows propagating uncertainty between scales. To optimize running times, a representative sampling of the homogenized quantities is adopted for the structural analysis. The paper is organized as follows: Section 2 addresses the proposed probabilistic two-scale numerical strategy; Section 3 describes the framework that extends the latter probabilistic numerical model for seismic fragility assessment of structures; Section 4 reports the application of the framework for structural and damage analysis of a case study, in which seismic fragility functions are found; and Section 5 reports the main findings and final remarks.

2. Probabilistic two-scale numerical strategy

A two-step numerical procedure able to consider geometrical, mechanical, and loading uncertainties is presented. The numerical strategy makes use of a classical first-order homogenization scheme: (i) the solution of the meso-scale problem; (ii) the meso-to-macro transition; and (iii) the solution of the macro-scale problem. The numerical framework relies on a direct homogenization approach, which involves solving a meso-mechanical problem at a meso-scale and deriving average field variables. This information is then carried out to the macro-scale to constitutively describe the behaviour of the structure. The two-step procedure has a stochastic nature and is incorporated into a comprehensive framework to produce seismic fragility curves, as illustrated in Fig. 1. This section is towards such steps that are part of the numerical model used in the structural analysis.

2.1. First step at a meso-scale level

The first step is performed at a meso-scale. A meso-mechanical problem is solved at an unit-cell level and average field variables are computed for the in- and out-of-plane responses. The problem is developed for the case of regular masonries in which periodicity is observed at both scales. In such cases, a single Representative Volume Element (RVE) can be defined, herein denoted as Ω_m. The kinematic description of the in-plane case assumes that the macroscopic strain tensor $\mathbf{E}$ is obtained as the volume average of the mesoscopic strain field ϵ_m at each point over the associated RVE:

$$\mathbf{E} = \frac{1}{V_m} \int_{\Omega_m} \boldsymbol{\epsilon}_{\mathbf{m}} \, dV \tag{1}$$

in which V_m is the volume of the RVE. The mesoscopic strain field can be decomposed into a macro-scale and meso-scale contribution

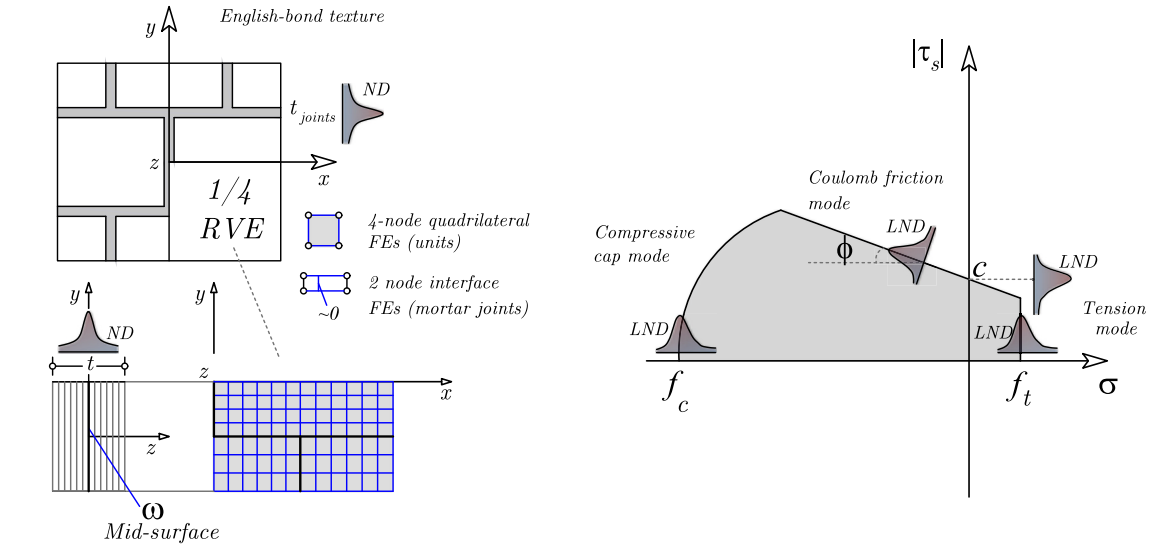

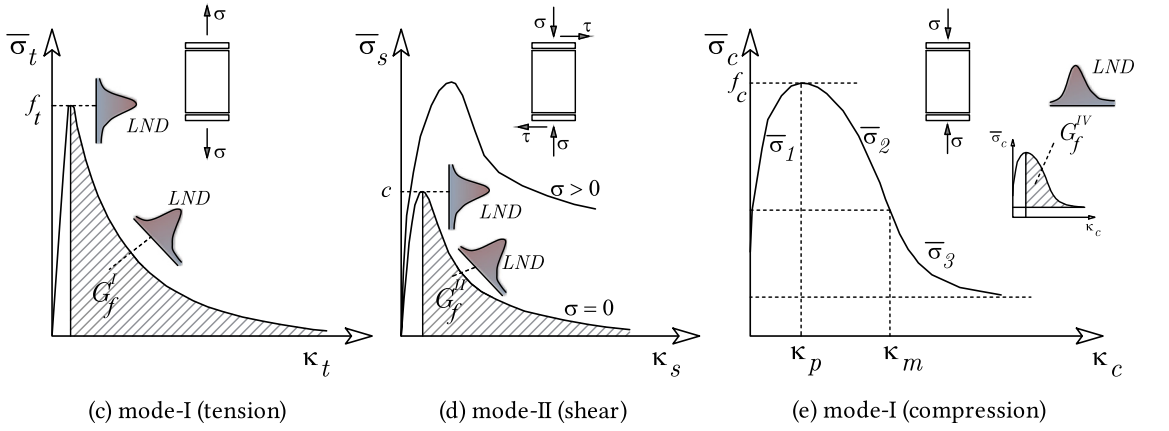

Fig. 2. Representative Volume Element (RVE) assumed at a unit-cell level, plasticity model and constitutive response adopted for mortar joints (ND, Normal distribution; LND, Log-normal distribution).

through an additive decomposition of the mesoscopic strain tensor $\delta\boldsymbol{\epsilon}_m = \delta\mathbf{E} + \nabla^s u_m$, in which $\delta\mathbf{E}$ is the applied constant strain tensor over the RVE and $\nabla^s u_m$ is the gradient of the fluctuation displacement field. The homogenized generalized stress is computed considering the mesoscopic stress field $\boldsymbol{\sigma}_m$ upon RVE equilibrium following the Hill–Mandel principle – energetic equivalence between macroscopic and mesoscopic works –, as follows:

$$\boldsymbol{\Sigma} : \delta\mathbf{E} = \frac{1}{V_m}\int_{\Omega_m} \boldsymbol{\sigma}_m \delta\boldsymbol{\epsilon}_m \; d\Omega \tag{2}$$

in which $\boldsymbol{\Sigma}$ is the macroscopic stress tensor. Following the assumed additive decomposition of the mesoscopic strain tensor, the macro-homogeneity principle can be written for any kinematic admissible δu_m:

$$\boldsymbol{\Sigma} : \delta\mathbf{E} = \frac{1}{V_m}\int_{\Omega_m} \boldsymbol{\sigma}_m \delta\mathbf{E} \; d\Omega + \frac{1}{V_m}\int_{\Omega_m} \boldsymbol{\sigma}_m \nabla^s \delta u_m \; d\Omega \tag{3}$$

Periodic boundary conditions are assumed to solve the Boundary Value Problem (BVP). Such consideration is extensively found in homogenization procedures for the study of masonry structures [63–67]. Due to the periodicity of the displacement fluctuations on the boundaries, the second term of Eq. (3) vanishes since the minimal kinematic constraint required to obtain an admissible mesoscopic generalized displacement fluctuation is null. Thence, the corollary of the Hill–Mandell principle is that the homogeneous macroscopic stress tensor $\boldsymbol{\Sigma}$ can be written as the volume average of the mesoscopic stress field $\boldsymbol{\sigma}_m$ over the RVE:

$$\boldsymbol{\Sigma} = \frac{1}{V_m}\int_{\Omega_m} \boldsymbol{\sigma}_m \, d\Omega \tag{4}$$

The variational principle and the use of periodic boundary conditions allow concluding that the external surface traction and body force field in the RVE are reactive terms over the imposed kinematic conditions. The macro-stress couples are obtained per unit of length and found through-the-thickness integration of the in-plane homogeneous macro-stresses. To solve the meso-mechanical problem, a two-dimensional unit-cell Finite Element (FE) model based on a Kirchhoff-plate theory method is adopted. It was presented in [40,68] using a deterministic approach and is herein extended for a probabilistic-based analysis.

The approach relies on a direct homogenization scheme, in which the BVP is solved upon a proper RVE that statistically embodies the masonry under study. Brick units are considered elastic and modelled through quadrilateral FEs. Mortar joints are considered inelastic and modelled through interface FEs. Material non-linearity is assumed to be lumped on mortar joints, see Fig. 2a. Such assumption is particularly adequate for strong unit masonry structures but, in the case of a weak unit–strong joint masonry type, units crushing can be represented by introducing an additional interface in the mid-span of each unit, as demonstrated in [40]. The linear elastic relation between the interface

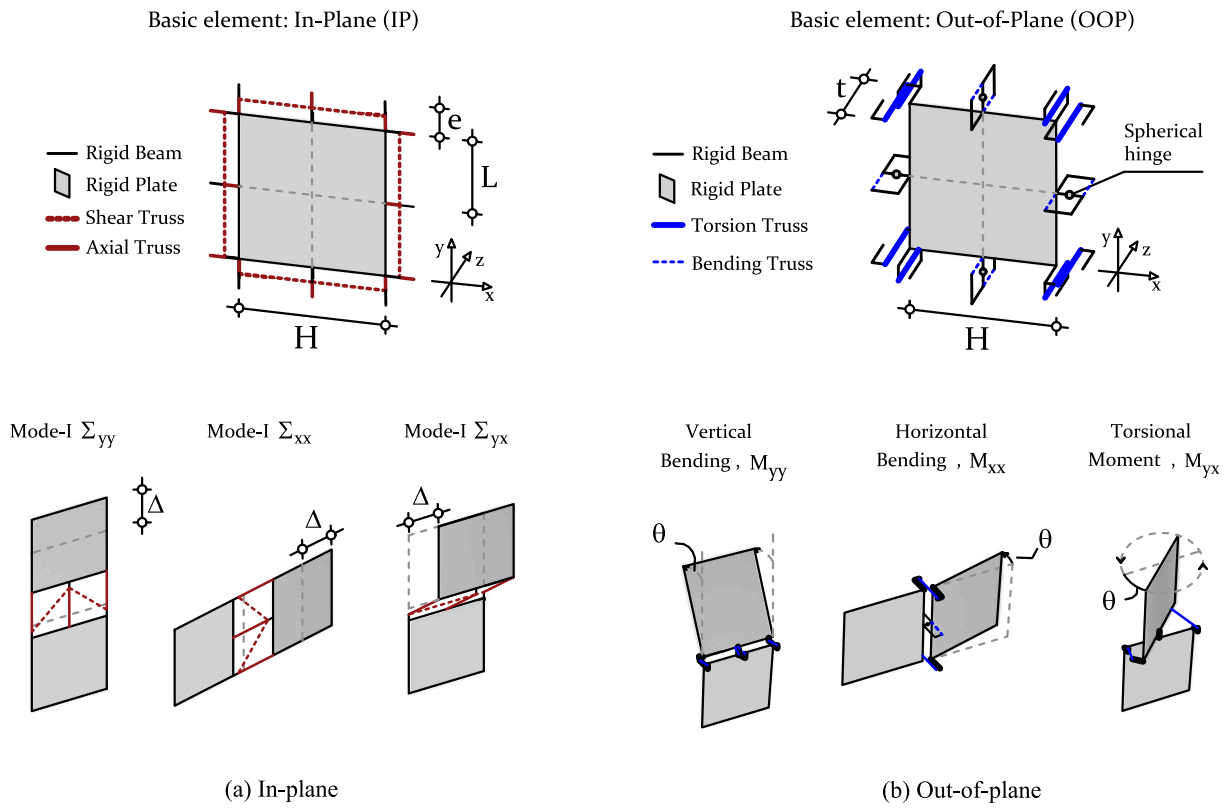

Fig. 3. Discrete macro-element model and corresponding Cauchy deformation modes.

generalized stresses and strains is given by $\boldsymbol{\sigma} = \mathbf{D}\boldsymbol{\epsilon}$, in which the stiffness matrix $\mathbf{D} = diag\{k_n, k_s, k_t\}$ (the subscript n refers to the normal and the subscripts s and t to the in-plane and out-of-plane shear components, respectively). These parameters are given by:

$$k_n = k_t = \frac{E_{brick}E_{mortar}}{t_{joint}(E_{brick} - E_{mortar})} \quad ; \quad k_s = \frac{G_{brick}G_{mortar}}{t_{joint}(G_{brick} - G_{mortar})} \tag{5}$$

in which E_{brick} and E_{mortar} are the Young's modulus of the brick unit and mortar, respectively; G_{brick} and G_{mortar} are the shear modulus of the unit and mortar, respectively; and t_{joint} is the thickness of the mortar joints. The so-called composite interface model [69,70] is adopted, which is able to reproduce fracture, frictional slip and crushing along the interface elements of the joints. It is defined by a convex composite yield criterion with three individual functions (see Fig. 2b) able to represent softening behaviour, i.e. a (i) a tension cut-off criterion designated as $f_{criterion,1}$ and defined in Eq. (6); (ii) a Mohr–Coulomb shear criterion designated as $f_{criterion,2}$ and defined in Eq. (7); and (iii) a cap in compression designated as $f_{criterion,3}$ and defined in Eq. (8).

$$f_{criterion,1}(\boldsymbol{\sigma}, \kappa_1) = \sigma - \bar{\sigma}_1(\kappa_1) \quad , \quad \bar{\sigma}_1 = f_t \exp\left(-\frac{f_t}{G^I_{ft}}\kappa_1\right) \tag{6}$$

The shear criterion (Fig. 2b, d) is given as:

$$f_{criterion,2}(\boldsymbol{\sigma}, \kappa_2) = |\tau| + \sigma \tan\phi(\kappa_2) - \bar{\sigma}_s(\kappa_2) \quad , \quad \bar{\sigma}_2 = c \exp\left(-\frac{c}{G^{II}_f}\kappa_2\right) \tag{7}$$

For the compression yield function (Fig. 2e) and using a matrix form:

$$f_{criterion,3}(\boldsymbol{\sigma}, \kappa_3) = \frac{1}{2}(\boldsymbol{\sigma}^T\mathbf{P}\boldsymbol{\sigma}) + \mathbf{p}^T\boldsymbol{\sigma} - \bar{\sigma}^2_3(\kappa_3) \tag{8}$$

Here, $\boldsymbol{\sigma}$ is the generalized stresses, f_t is the interface bond strength, c is the interface cohesion, ϕ is the friction angle; $\mathbf{P}$ is a projection diagonal matrix and $\mathbf{p}$ a projection vector based on material parameters [69]; $G^I_{f_t}$, G^{II}_f are the mode-I and mode-II fracture energy terms, respectively; $\bar{\sigma}_1$, $\bar{\sigma}_2$ and $\bar{\sigma}_3$ are the effective stresses of each the adopted yield functions governed by the internal scalar variables κ_1, κ_2 and κ_3, respectively. The typical compression hardening/softening law $\bar{\sigma}_3(\kappa_3)$ is composed of three branches (Fig. 2e), which are in agreement with the $\bar{\sigma}_{c1}$, $\bar{\sigma}_{c2}$ and $\bar{\sigma}_{c3}$ laws defined in [69]. Note that the subscripts i, m and r for both the yield stress value and scalar κ indicates the initial, medium and residual values, respectively. The compression fracture energy G^I_{fc} corresponds to a material input parameter of the model and allows computing the residual strength value $\bar{\sigma}_r$ (from the peak $\bar{\sigma}_p$ one).

Probability distribution functions are assigned to each input parameter, in specific to both geometric and material properties. If $\mathbf{X}$ defines the discrete set of input random system variables X_i, then one can write the following:

$$\mathbf{X} = \{E_{brick}, E_{mortar}, f_t, G^I_{f_t}, f_c, G^I_{f_c}, c, G^{II}_f, \phi, t_{joint}, t\} \tag{9}$$

in which $\forall X_i \in \mathbf{X} : X_i = f(x)$. Note that, although upper letters are typically used to represent random variables, the corresponding lowercase letters for geometrical and strength related material parameters were adopted to follow the classical structural mechanics notation. The sampling of random variables (RVs) is achieved by the LH method. It allows a more rational selection of the RVs sample than the MC technique [71,72], as a stratified technique allows avoiding overlapped simulations [73]. To this aim, it is necessary to define: (i) a probabilistic distribution function (PDFs) for each RV and the correlation matrix; and (ii) the dimension of the probabilistic sample, i.e. the desired number of simulations N_{simul}. Once these two steps are performed, the solution of the mesoscopic BVP is found for each input sample. The process is repeated N_{simul} times, hence finding N_{simul} homogenized $\Sigma - E$ and $M - \chi$ quantities.

2.2. Second step at a macro-scale level

A discrete-based numerical model is adopted at a macro-scale. Masonry is modelled as a discrete media. The basic macro-element is composed by a quadrilateral rigid plate with deformable FE-trusses at its interfaces. Those trusses govern both in- and out-of-plane deformation and damage (Cauchy deformation modes of Fig. 3) within a decoupled

characterization. Therefore, the orthotropy and full-softening response of masonry can be represented and the significant computational costs of continuous FE-models for non-linear dynamic problems circumvented. The mass of the system is embodied by the quadrilateral rigid plates through an equivalent material density and within a consistent mass matrix approach.

The discrete macro-element was implemented in software ABAQUS [74]. As demonstrated in [75], the homogenized constitutive relationships can be reproduced with good accuracy through the concrete damage plasticity (CDP) model. Such plasticity model is applied to the macro-interfaces only (trusses) and requires stress–strain curves as input. Meso-to-macro steps are performed to guarantee the correct upscaling of the homogenized $\Sigma - E$ and $M - \chi$ curves: (1) the scaling, and (2) the fracture energy regularization. Both are dependent on geometric parameters, i.e. H, e, L, t, (Fig. 3).

The in-plane response is directly obtained from the $\Sigma - E$ curves. For the out-of-plane trusses, i.e. bending (BTruss) and torsion (TTruss), the macroscopic M quantities are converted in stress values according to Eq. (10):

$$\sigma_{BTruss} = \frac{M}{e A_{BTruss}} \quad ; \quad \sigma_{TTruss} = \frac{M}{H A_{TTruss}} \tag{10}$$

Here, M is the bending moment per unit of interface length, H the length of each quadrilateral panel, and t is the thickness of the wall. The bending truss area is given by $A_{BTruss} = H(L + \frac{e}{2})$ and the torsional truss area given by $A_{TTruss} = \frac{eH}{2}$, in which e is the gap between macro-elements (assumed as 20 mm) and $L = \frac{H}{2}$ is the influence length of each truss.

The stress–strain curves for trusses are regularized by affecting the elastic stiffness and fracture energy terms. Regularization is necessary to correctly identify the elastic stiffness of trusses and to guarantee the solution objectivity in non-linear problems. The elastic stiffness of each truss is found by assuring the elastic energy equivalence between the discrete model and an equivalent Cauchy homogeneous plate. The Young's moduli of the in-plane trusses are given as:

$$E_{ii}^{IP\,axial\,truss} = \frac{\bar{E}_{ii} e}{2(2L + e)} \quad ; \quad E_{ij}^{IP\,shear\,truss} = \frac{\bar{G}_{ij} H^2}{4e(2L + e)} \qquad i, j = \{x, y\} \tag{11}$$

For the out-of-plane bending and torsional responses, the Young's moduli are calculated as:

$$E_{ii}^{BTruss} = \frac{\bar{E}_{ii} t^4 H}{24e(1 - \nu^2)(H + e) e A_t} \quad ; \quad E^{TTruss} = \frac{2\bar{G} t^4}{3H^2 e(2L + e)} \qquad i, j = \{x, y\} \tag{12}$$

In which $\bar{G} = \frac{\bar{E}_{ii}}{2(1+\nu)}$ is the homogenized shear modulus. By correcting the strain axis to calibrate the elastic stiffness value, the post-peak curve strains are also affected and regularize the fracture energy. A concise description was given herein, being the reader referred to [75,76] for further insights on the deterministic-based formulation.

3. Proposed framework for seismic fragility assessment

The two-step numerical procedure is able to account with different sources of uncertainty and can, moreover, be integrated within a framework for fragility or reliability analysis. Herein, and observing the model as a structural analysis tool, further details are given on how the uncertainties are propagated. Then, the possibility of applying the numerical model within a damage analysis is also provided, in specific within the so-called PBEE methodology for the seismic vulnerability assessment of masonry structures.

3.1. Meso-to-macro scale: propagation of uncertainty

System uncertainty is represented by considering variables to be random (RVs) [77,78]. Defining simple and non-stationary statistical distribution functions to RVs seem appropriate in the majority of structural problems [79,80]. The probabilistic model code JCSS (2011) [62] addresses the latter by offering recommendations on statistical distributions and parameters for several construction materials (as concrete, timber, and masonry). Variables concerning the loading, masonry material properties, and the structure's geometry can then carry uncertainty. In particular, as referred in Section 2.1, the following mesoscopic variables are eligible to carry uncertainty:

$$\mathbf{X} = \{E_{brick}, E_{mortar}, f_t, G_{f_t}^I, f_c, G_{f_c}^I, c, G_f^{II}, \phi, t_{joint}, t\} \tag{13}$$

in which $\forall X_i \in \mathbf{X} : X_i = f(x)$, being, so far, assumed that $f(x)$ follows either a normal (ND) or log-normal distribution (LND). Nonetheless, since the dimension of $\{X\} = \{X_1, X_2, X_3, \ldots, X_{i+1}\}$ has a direct effect on the computational processing time, a sensitivity analysis may be performed beforehand to reduce the random space dimension.

In presence of uncertainty, sampling methods are generally used to establish the set of RVs and to compute the failure probability of a system. Methods such as the Monte-Carlo (MC) or Latin-Hypercube (LH) [45,55,81] are generally adopted for both non-linear and large-scale problems. MC [82] follows a random sampling approach and it is conceptually more straightforward, but demands higher computational costs if acceptable confidence limits are desirable. LH adopts a rational selection of the RVs set through a stratified sampling technique that avoids overlapped simulations [73], hence lessening the computational effort in respect to crude MC [72].

A LH sampling method within an inverse transform method is adopted here (based on [73]). The sampling allows deriving a set of N_{simul} grouped RVs values of the array $\mathbf{X}$, being N_{simul} provided by the analyst. Since input variables can be correlated, the use of a non-identity covariance matrix is suggested and convenient. Note that using representative correlations allows guaranteeing that the simulated responses are physically plausible. A correlation measure based on the Pearson product-moment coefficient $\rho_{i,j}$ (subscripts i and j denote two given variables) was assumed.

The propagation of uncertainty from the meso- to the macro-scale is conducted by upscaling $N_{propagated}$ homogenized $\Sigma - E$ and $M - \chi$ curves. The number of propagated curves ($N_{propagated}$) is lower than the total number of the random homogenized quantities computed N_{simul}, i.e. $N_{propagated} \subset N_{simul}$. This is a paramount advantage of the proposed structural analysis model, as it allows to significantly reduce the number of analyses performed at a macro-scale. Towards the latter, homogenized curves that represent the full stochastic meso-scale content are properly found. To this aim, curves that statistically represent the random response using five percentile are found: the 5%, 25%, 50% (median), 75%, and 95% percentiles. Furthermore, one may also ensure that such representative homogenized curves are correlated. The application of this step is demonstrated in Section 4.2.3.

3.2. Structural non-linear analysis

The proposed numerical model can be used at a macro-scale for the structural seismic assessment of masonry structures, either through non-linear quasi-static (Pushover) or non-linear dynamic analysis. Here, we address the particular case of non-linear incremental dynamic analysis (IDA). IDA allows a better estimation of dissipated energy, resulting forces and overturning moments than static approaches [83], albeit requiring significantly higher computation costs. The seismic capacity evaluation through IDA curves requires: (i) an appropriate strong motion intensity measure (IM) [84]; and (ii) an appropriate engineering demand parameter (EDP) [85,86]. Dynamic analyses are then conducted considering the propagated homogenized data

($N_{propagated}$). Loading uncertainty is also acknowledged by providing different ground motions scaled for each IM level.

Peak-ground acceleration (PGA), velocity (PGV), and displacement (PGD), the Arias intensity, and the Housner Intensity are examples of IMs. The selection of the most adequate IM is still debatable, but it should include concerns related to the adopted hazard model, the system (structural or not-structural) under analysis and the available data [87]. Several studies report different optimal IMs for a performance-based analysis, either for new and existing structures [88,89]. The decision of the IM is paramount, as the series of non-linear dynamic analyses are carried for different IM levels. Furthermore, the so-called Engineering Demand Parameter (EDP) needs to be established to assess the response of the system. As referred in [83], the EDP selection depends on the performance target and on the type of system under investigation. Possible EDPs include story drifts; rotation values; total or inelastic deformations; floor accelerations or velocities; internal forces of elements; strength degradation or energy dissipation values, among others. Lastly, IDA curves can be computed to describe the structural response in terms of EDP and IM levels for the ground motions. Note that IDA analysis offers a comprehensive insight into the seismic response of structural system, but allows also constructing important decision-tools, such as fragility or vulnerability (if losses are estimated) curves.

3.3. Damage analysis

The possibility of adopting the proposed probabilistic-based model within a damage analysis is provided. The strategy is applied to obtain seismic fragility curves through IDA analysis, for which damage regions and corresponding limit state (LS) levels may be defined. Fragility curves are here obtained by fitting the discrete data using a cumulative log-normal probabilistic distribution, as it was demonstrated to be an appropriate choice [83,90,91]. Such curves relate the POE a given damage threshold as a function of the strong ground motion IM. Mathematically, the formal definition is gen as:

$$F_{LS}(IM) = P[EDP \geq EDP_C \mid IM] \tag{14}$$

in which $F_{LS}(IM)$ is the fragility at a given IM and for a limit state (LS) with an associated capacity limit for the engineering demand parameter EDP_C. Note that according to Eq. (14) it is assumed that if the EDP_C is reached then the LM is violated, but other formal definition that considers it as the ultimate safe limit are also found in literature [92]. A log-normal fragility curve is determined for a generic LS and the estimation of the log-normal parameters is herein achieved using the maximum-likelihood method, as it provides accurate estimations of $\hat{\theta}$ and $\hat{\beta}$ ($\hat{}$ denote an estimated parameter) [91].

The Maximum-likelihood method (MLM) computes the estimated moments $\hat{\theta}$ and $\hat{\beta}$ through a maximization problem on the likelihood of the predicted data in fitting the expected one. Prior to the optimization step itself, the computation of the number of events n_c (out of the total N_{events}) whose EDP value exceeded the limit value δ_{LS} is needed, for each defined LS and accounting with all the IM levels. By adopting a binomial distribution, the probabilities of collapse can be computed from Eq. (15):

$$P[n_c \ out \ of \ N_{events} \mid IM = x] = \binom{N_{events}}{n_c} p^{n_c} (1 - p_i)^{N_{events} - n_c} \tag{15}$$

in which p is the probability of reaching/exceeding the LS at $IM = x$. After repeating this process for all the IM values, the likelihood of the entire set of analysis is given as the product of the individual likelihoods. In this regard, the optimization function is written over the total likelihood (the sum of the individual likelihoods) and, owing to a mathematical convenience [91], in a logarithmic form and reads as given in Eq. (16). Such optimization problem can be solved using a Nelder–Mead simplex algorithm (fminsearch function in MATLAB was adopted) for each LS, and the estimated log-normal distribution parameters $\hat{\theta}$ and $\hat{\beta}$ are computed.

$$\{\hat{\theta}, \hat{\beta}\} = \arg\max_{\theta,\beta} \sum_{j=1}^{m} \left[n_c \ln\left(\Phi\left(\frac{ln\left(\frac{x}{\theta}\right)}{\beta} \right) \right) + (N_{events} - n_c) \ln\left(1 - \Phi\left(\frac{\ln\left(\frac{x}{\theta}\right)}{\beta} \right) \right) \right] \tag{16}$$

4. Application of the framework

The proposed framework is applied to the seismic fragility assessment of an English-bond masonry benchmark. Each of the conducted stages of the framework are addressed in detail, and encompass the meso-mechanical characterization of masonry, propagation of uncertainty, and the structural and damage analyses performed at a macro-scale. The latter steps are depicted with detail in Fig. 4.

4.1. Case study: LNEC brick masonry benchmark

An English-bond brick-house mock-up [93] is selected to serve as benchmark for the application of the framework. The structure is composed of three walls in a U-shaped plan arrangement. Main façade (East plan) presents a gable wall, which is linked with two transversal abutment walls (North and South plans). Walls are made of clay brickwork, within an English-bond arrangement, with 235 mm of thickness. Clay brick units have nominal dimensions of $235 \times 115 \times 70$ mm^3 and are laid and bound together by mortar joints with a thickness ranging from 15 to 18 mm. The geometrical features are depicted in Fig. 5. The brick mock-up was tested up to collapse in a shaking table under a unidirectional seismic loading. The seismic input was applied in a perpendicular direction (E-W) to the main façade. Preceding experimental observations [93] and numerical analysis [76] on its dynamic response showed that the governing failure mode is given by the out-of-plane collapse of the tympanum of the gable wall. Hence, the seismic fragility is assessed accounting with such collapse mode.

4.2. Stochastic meso-mechanical characterization of masonry

4.2.1. Sensitivity study of the input parameters

The random space dimension $\mathbf{X} = \{X_1, X_2, X_3, \ldots, X_{i+1}\}$ of the system has a direct effect on the computational processing time. The input variables for the mesoscopic model are gathered in Table 1. Expected values and CoV terms follow experimental data [93] and the recommendations from JCSS (2011) [62], when applicable. The probabilistic distributions of RVs have been assumed to follow a Log-Normal (LN) distribution when related with mechanical parameters of the masonry, and a Normal (N) distribution when related to geometric parameters. Such assumptions are generally followed, as demonstrated in [94]. Masonry density ρ and Poisson's coefficient ν are assumed to be deterministic owning its low experimental variability [93].

A sensitivity analysis was conducted to evaluate the relative importance of each parameter on the OOP homogenized quantities: horizontal (M_{xx}), vertical (M_{yy}) and torsional (M_{xy}) bending moment–curvature relationships. Such constitutive laws are provided from the meso-scale analysis (described in Section 2.1) on a Representative Volume Element (RVE) of the English-bond masonry of the case study (Fig. 3). Two meso-scale simulations were performed for each studied variable X_i by considering the lower (5% percentile) and upper-bounds (95% percentile). For the remaining RVs, the median value was attributed. This process is repeated for each X_i and a total of 23 analyses ($2X_i + 1$) were simulated. Results are assembled through tornado diagrams, see Fig. 6. Variables are positioned in the ordinates and the bar length represents the consequence of changing the variable to a lower-

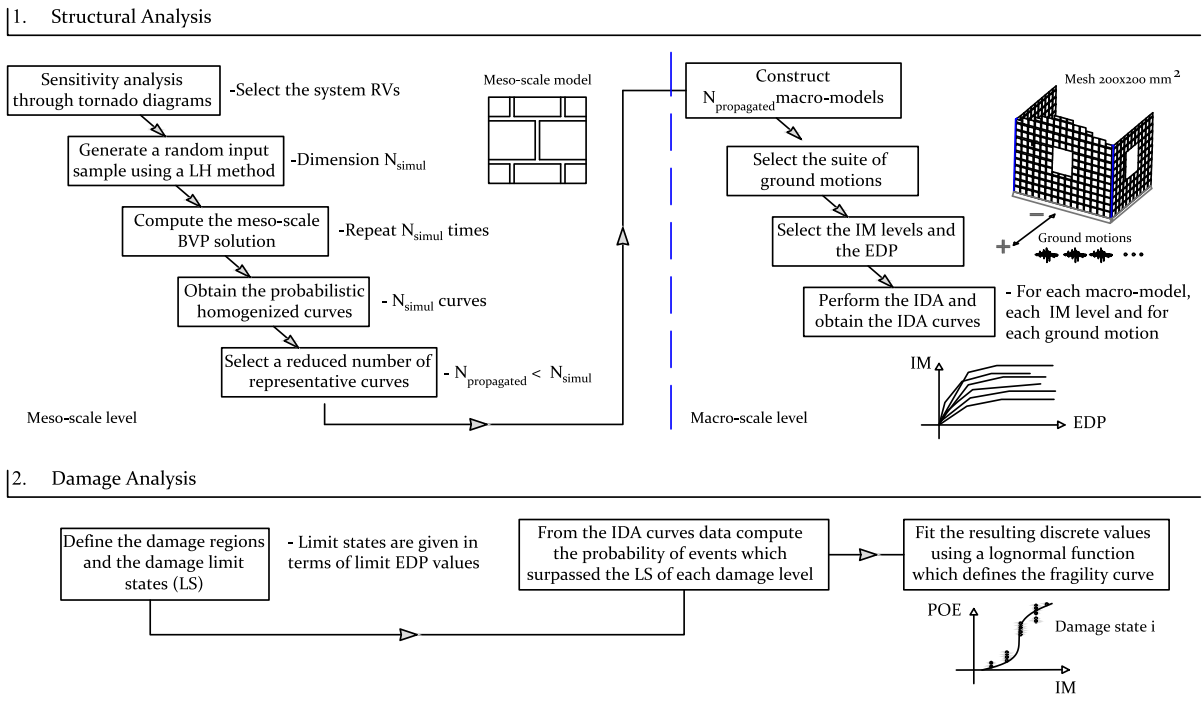

Fig. 4. Proposed methodology to use the two-step numerical procedure.

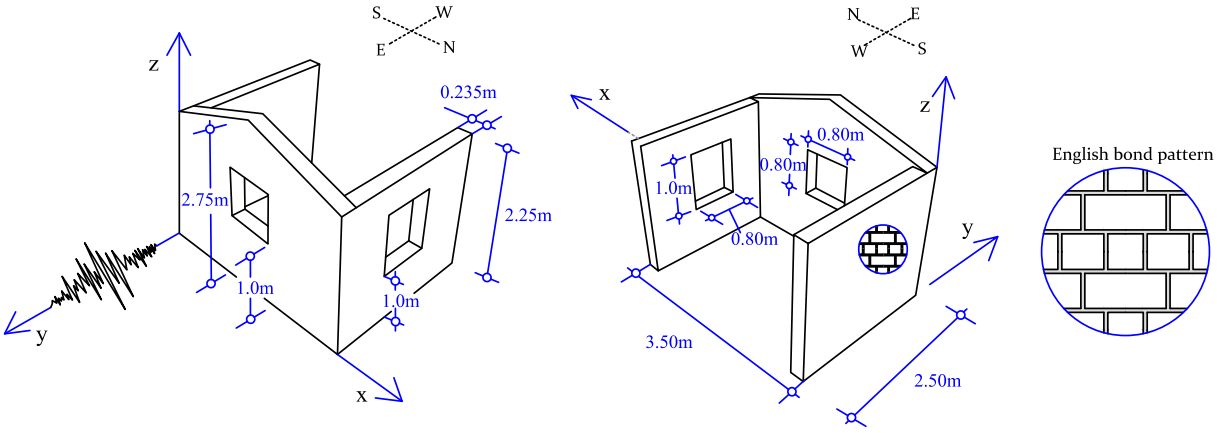

Fig. 5. Selected case study: the LNEC brick-house benchmark.
Source: Adapted from [76].

and upper-bound with respect to the base (median). Most influential variables are placed in the top of the chart and follow a descending order. Since both material and geometric parameters are considered as RVs, one may expect that differences are accountable on the maximum moment capacity and on the $M-\chi$ curve shape. Accordingly, a local and global control parameter was assumed for the (M_{xx}), (M_{yy}) and (M_{xy}) curves, i.e. the peak moment value and the total stored energy, respectively.

Results indicate that parameters as the cohesion (c), tensile strength (f_t) and thickness (t) govern both the local (peaks) and global (energy) meso-response. In converse, parameters related with the compressive regime seem to have a negligible effect. These findings are in agreement with experimental evidences for weak mortar masonries, in which both tensile and shear regimes tend to govern the out-of-plane behaviour [95]. Hence, compressive strength f_c and fracture energy $G^I_{f_c}$ were defined as deterministic variables. Thus, a total of nine variables were defined to be random and carry the uncertainty of the systems:

$$\mathbf{X} = \{E_{brick}, E_{mortar}, f_t, G^I_{f_t}, c, G^{II}_f, \phi, t_{joint}, t\} \quad (17)$$

Table 1
Statistical properties of the RV for sensitivity study.

X_i	Statistical distribution	$E[X_i]$	$CoV[X_i]$
E_{brick} (N/mm^2)	LN	11000	29% [93]
E_{mortar} (N/mm^2)	LN	3000	25% [62]
$f_{c,mortar}$ (N/mm^2)	LN	2.48	17% [62]
$f_{t,mortar}$ (N/mm^2)	LN	0.105	25%
$G^I_{f_c}$ (N/mm)	LN	3.97	17%
$G^I_{f_t}$ (N/mm)	LN	0.012	25%
G^{II}_f (N/mm)	LN	0.05	25%
c (N/mm^2)	LN	0.2	40% [62]
ϕ (degrees)	LN	30	19% [62]
t (mm)	N	235	5% [93]
t_{joint} (mm)	N	15	20% [93]

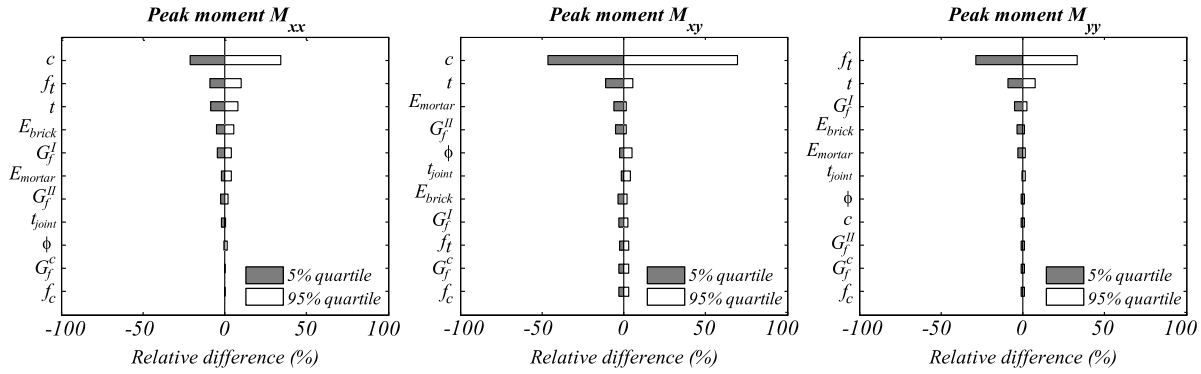

(a) local parameter: peak strength value

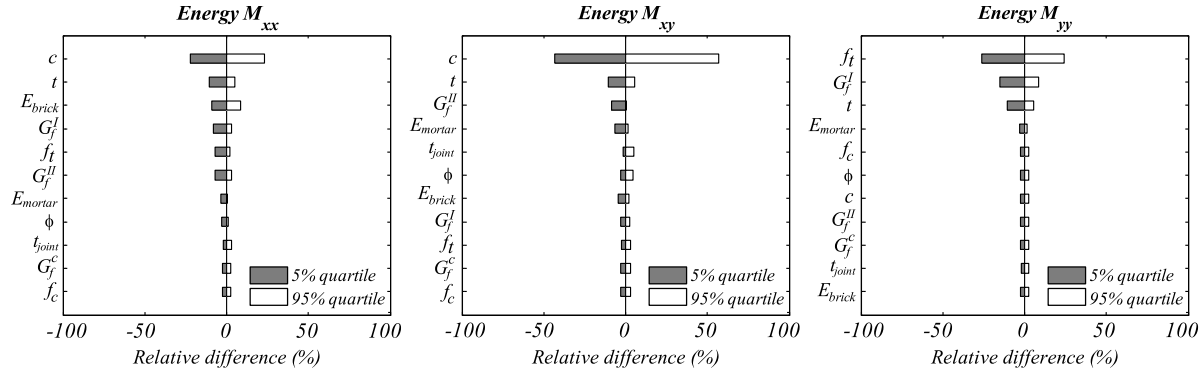

(b) global post-peak parameter: stored bending energy

Fig. 6. Tornado diagrams for the eleven random variables (RVs) of the system.

It is stressed that such material information is generally unavailable as masonry's experimental characterization is only feasible in some studies. Therefore, literature on alike masonries may provide valuable recommendations. It is suggested that: (i) elastic and strength properties can be found using the so-called masonry quality index [96]; and (ii) non-linear properties of masonry and unit-mortar interface to be found following non-destructive tests [46], confined compression tests [97], or using general recommendations for masonry [69] whose representativity can be arguable depending on the masonry type.

4.2.2. Latin-hypercube sampling (LHS)

A LHS method within an inverse transform method is chosen (Section 3.1). The sampling process has a set size given as $N_{simul} = 2000$. A non-identity correlation matrix was considered since some RVs are correlated. This allows obtaining a meaningful sample of values and restrict the solution to physically plausible responses. The built-in LHS tool of MATLAB was used, which makes use of a correlation measure based on the Pearson product-moment coefficient ρ_{ij} (subscripts i and j denote two given variables). Table 2 reports the parameters adopted (namely the covariance matrix, see [73]), which are fully-based on expert judgment. Only null (independent variables) and positively correlated variables were considered, and spatial variability disregarded. The theoretical statistical distribution and the histograms obtained after the LHS are shown in Fig. 7 for each RV, in which a good match between the generated and expected distribution curves was found.

4.2.3. Propagation of uncertainty: meso-to-macro scale

From the sample obtained from the LH method, a total of $N_{simul} = 2000$ simulations were performed, and results ensure the variability of the system material, mechanical and geometrical parameters. Each generated sample serves as input for the BVP at the meso-scale and, by repeating this process for every sample, a total of 2000 homogenized stress–strain and moment–curvature curves were derived, as depicted in Fig. 8. Large variability of the meso-scale response is clear, partly explained by the adopted high CoV values for the most critical parameters. A convergence test was performed to assess the adequacy of the number N_{simul}.

Table 2
Target correlation matrix adopted between the RVs.

	E_{brick}	E_{mortar}	f_t	$G_{f_t}^I$	c	G_f^{II}	ϕ	t_{joint}	t
E_{brick}	1.0	0.4	0.2	0.2	0.2	0.2	0.2	0.0	0.0
E_{mortar}		1.0	0.8	0.6	0.6	0.4	0.2	0.0	0.0
f_t			1.0	0.6	0.6	0.4	0.2	0.0	0.0
$G_{f_t}^I$				1.0	0.6	0.4	0.2	0.0	0.0
c					1.0	0.6	0.2	0.0	0.0
G_f^{II}						1.0	0.2	0.0	0.0
ϕ		sym					1.0	0.0	0.0
t_{joint}								1.0	0.2
t									1.0

Fig. 9 shows that the mean of the generated peak moment of the homogenized (M_{xx}), (M_{yy}) and (M_{xy}) curves remain below the defined tolerance of 5% (in respect to the last simulated mean value) for an $N_{simul} = 500$. This indicates that $N_{simul} = 2000$ seems a conservative choice (note that $M-\chi$ curves are integrated from $\Sigma-E$ curves; hence the latter results are disregarded).

Aiming at reducing the number of simulations performed at a macro scale, the data from each homogenized quantity was analysed and the five principal percentiles filtered. The main purpose is the definition of five deterministic models that holistically represent N_{simul} different samples. The latter step got inspiration from [12], where representative

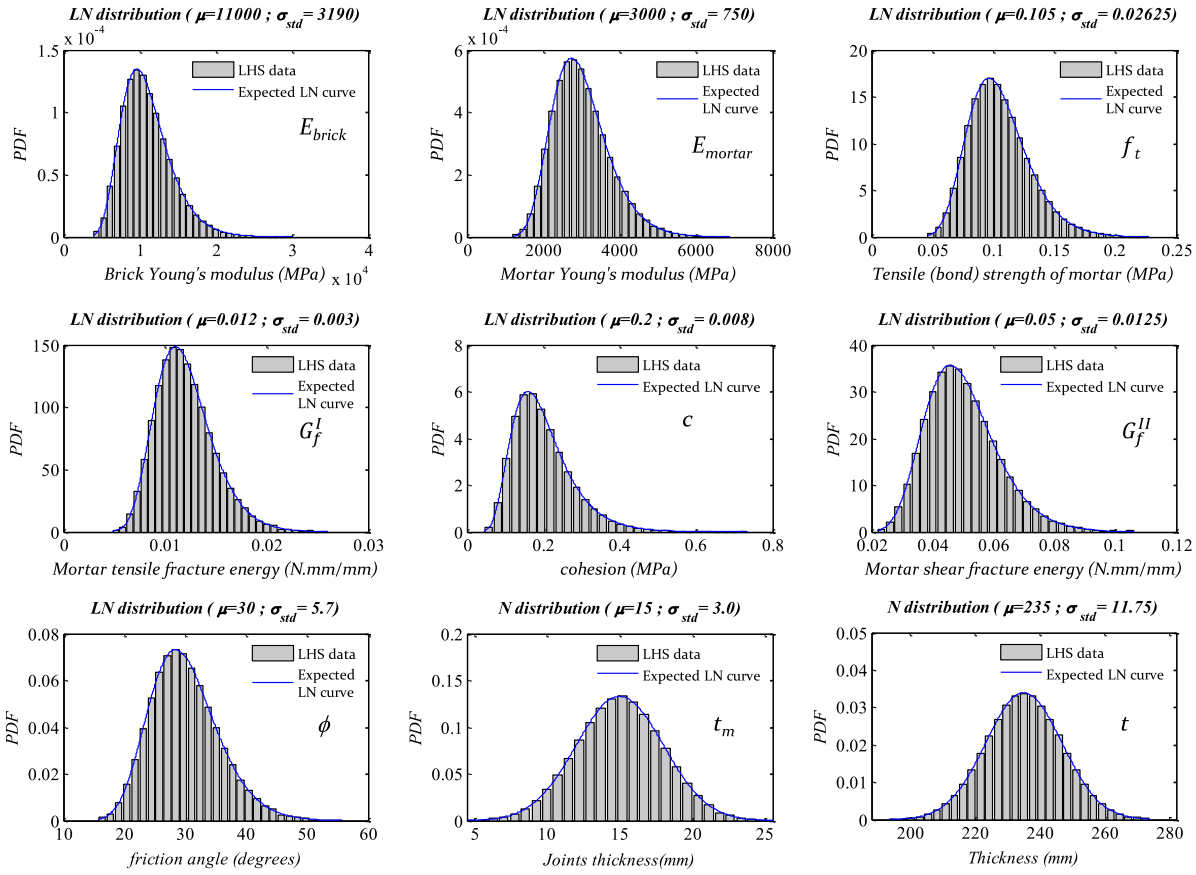

Fig. 7. Distribution for each RV generated through Latin Hypercube technique $N_{simul} = 2000$.

$M - \chi$ were used as input for hinges with concentrated plasticity for a frame-based model applied to reinforced-concrete structures. Nonetheless, combining the percentiles curves found for each homogenized quantity and assuming that outcome from the same input may be unrealistic. In other words, the sample that originates the maximum (M_{xx}) peak can differ from the one which originates the maximum (M_{xy}) and (M_{yy}) values. This is especially critical in a multivariate system, whereas the relative importance of each variable is more diluted and an obvious correspondence between models is hardly found. Bearing this in mind, a correlation test between the homogenized quantities being combined is mandatory. The correlation assessment was conducted via q-q (quantile–quantile) plots and results are addressed in Fig. 10.

Again, both a local and global parameter that characterizes the OOP homogenized quantities were accounted, namely the peak moment value and the stored bending energy. Likewise, only OOP quantities were considered to avoid redundancy, as moment are obtained from the stress quantities ($M_{xx} - \Sigma_{xx}$, $M_{xy} - \Sigma_{xy}$ and $M_{yy} - \Sigma_{yy}$). Fig. 10 demonstrate a quasi-perfect positive correlation between homogenized quantities (a Pearson linear correlation coefficient of 0.99) and within a confidence level of 95%. This supports the validity of filtering five models directly from the percentiles of the total random sample N_{simul}.

The uncertainty propagation between meso- and macro-scale is guaranteed by the five representative models plotted in Fig. 11. These are designated according to the corresponding percentiles, i.e. model P5%, model P25%, model P50%, model P75% and model P95%. Note that such an assumption is especially convenient since it reduces drastically the computational cost at a macro-scale and without lose of the representativeness of the simulations performed at a meso-scale.

4.3. Stochastic structural analysis

4.3.1. Random loading input using artificial accelerograms

Current code guidelines acknowledge the use of either real or artificial accelerograms. In regions where a significant set of ground-motion records of damaging earthquakes is unavailable, the use of real earthquakes is difficult. Furthermore, each record has its own wave characteristics contents, which makes the occurrence of a similar seismic event unlikely. Artificial accelerograms pose higher practicability and were adopted, as a significant number of random accelerograms, code-compliant with design response-spectrum, can be easily generated through existing tools [54,98,99]. Seven stationary signals were generated using SIMQKE_GR [98] and are given in Fig. 12. However, it should be noted that the debate over the use of artificial and real accelerograms is beyond the scope of this study. Real accelerograms can be certainly a viable option when applying the proposed framework.

Seven is the minimum number required by Eurocode 8 [49] to allow observing the mean structural response. Non-stationary signals (in amplitude and frequency content) were produced considering that: (1) the envelope function has a trapezoidal shape [100]; (2) total duration of 35 seconds, i.e. an intense phase with 30 seconds and a rise and decay phases with 5 seconds duration; (3) signals were high-passed in the frequencies range of 0.2–40 Hz and filtered using a cosine function to attenuate potential accelerations drifts; and (4) the resulting artificial accelerograms are compatible with the elastic response spectrum for an earthquake type-1 (far-fault earthquake) by Eurocode 8 [49], with 475 years for returning period P_n and 3% viscous damping ($\xi = 3\%$), see Fig. 12. This spectrum was found considering the parameters suggested by the Portuguese National Annex for the region

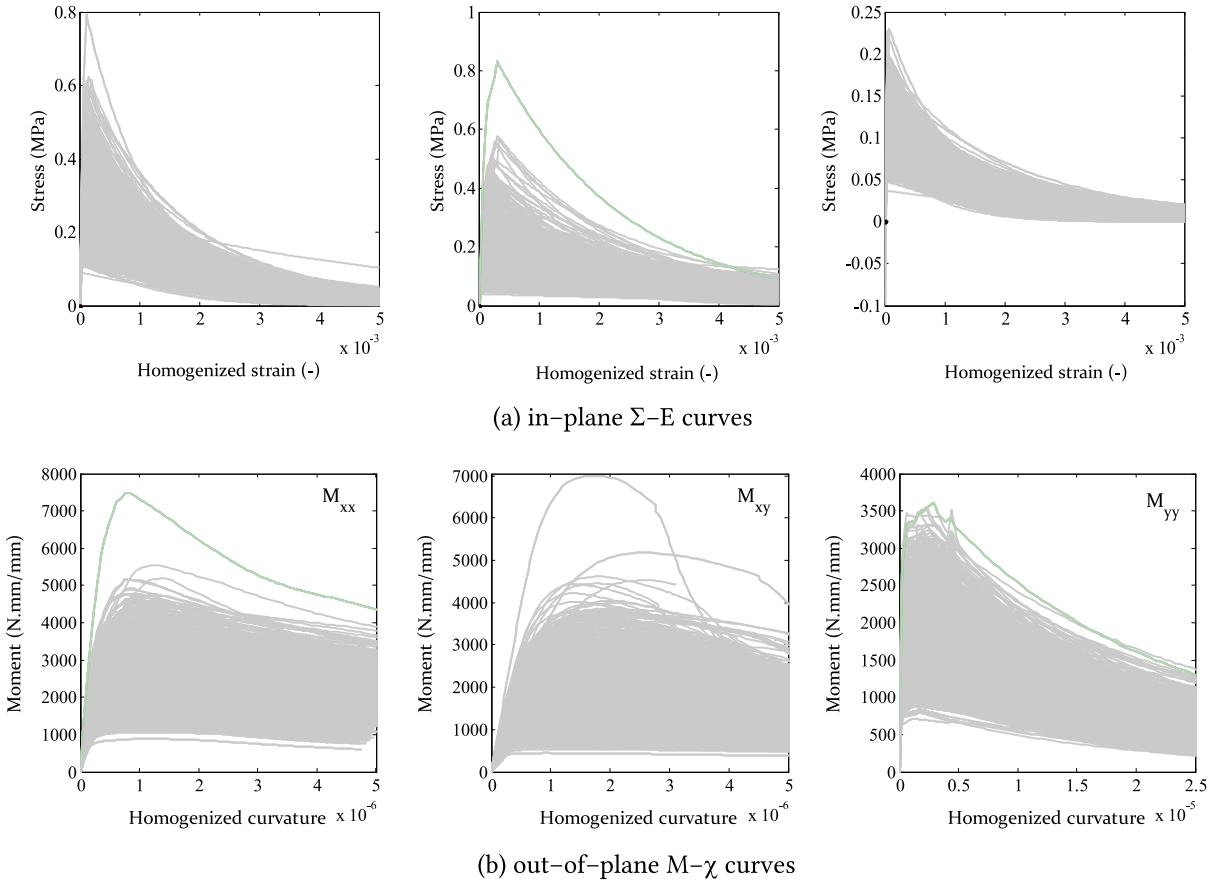

Fig. 8. Homogenized curves from $N_{simul} = 2000$ meso-scale simulations.

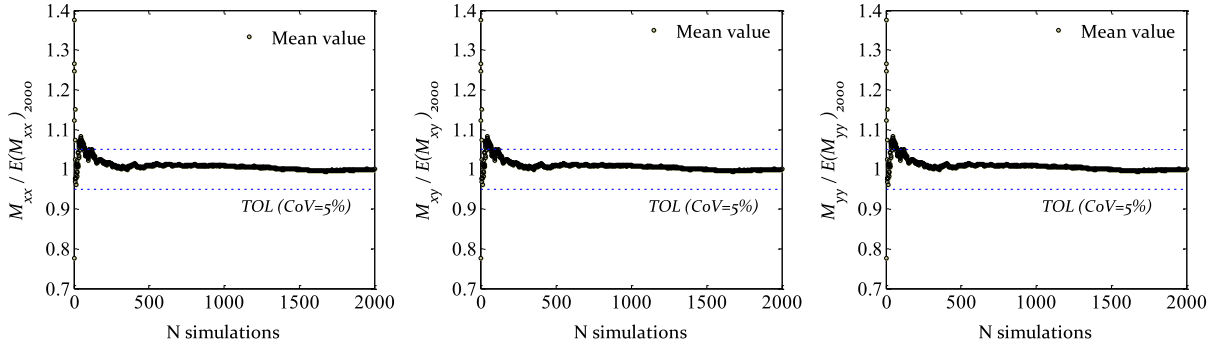

Fig. 9. Convergence tests performed for the obtained peak values of the (M_{xx}), (M_{yy}), and (M_{xy}) quantities during the $N_{simul} = 2000$ simulations performed.

of Lisbon: importance factor $\gamma_I = 1.0$ (Class B buildings); a reference peak ground acceleration of $a_{gr} = 1.5$ m/s^2; and a soil type A (rock, soil factor $S = 1$). Such values were hypothetical assumed aiming the application of the framework.

4.3.2. Incremental dynamic analysis (IDA)

IDA curves are computed from dynamic analyses by relating EDP-IM parameters [101]. Several grouping methods can be employed to effectively describe the EDP-IM space and determine the seismic demand. For instance, singe/multiple strip analysis [102] that use accelerograms scaled to match the desired IM level, and cloud methods, in which a set of scaled or unscaled ground motions appearing at arbitrary non-identical IM levels allows to obtain a cloud like shape of EDP-IM pairs. For a deeper discussion on other possible methods, the reader is referred to [92]. In this study, IDA is however adopted since authors agree that fragility is easily understood since failure can be promptly traced on a record-to-record basis [92,101].

As IM, ground-based specific measures (PGA, PGV and PGD) are practical, albeit lack robustness for long-period structures [103]. Still, PGA is largely adopted by current design codes for both hazard and motion attenuation relationships. Moreover, PGA was adopted in the reference experimental data [93], which enforces its convenience. Regarding the EDP, the maximum out-of-plane displacement component at the top of the gable wall (δ_{EDP}) was assumed. A displacement-based EDP is generally adopted within analytical-based fragility curves for URM structures [56,104–106] and/or in seismic URM buildings seismic provisions, for instance in FEMA 368 [107]. The seven artificial accelerograms were scaled according to nine IM levels, ranging from $0.1g$–$0.9g$ and with a periodicity of $0.1g$ (PGA levels). By recalling that uncertainty is represented at the macro-scale by five macro-models

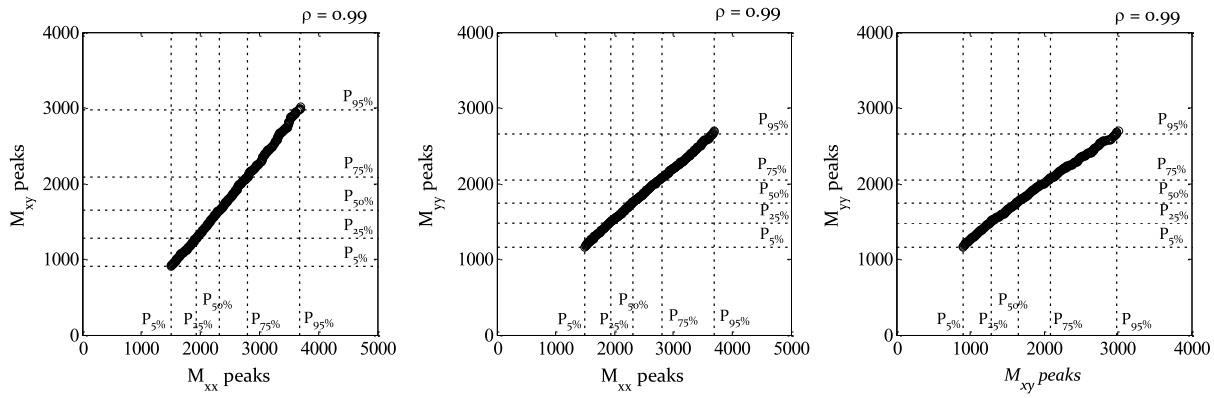

(a) q–q plots considering the peak moment values

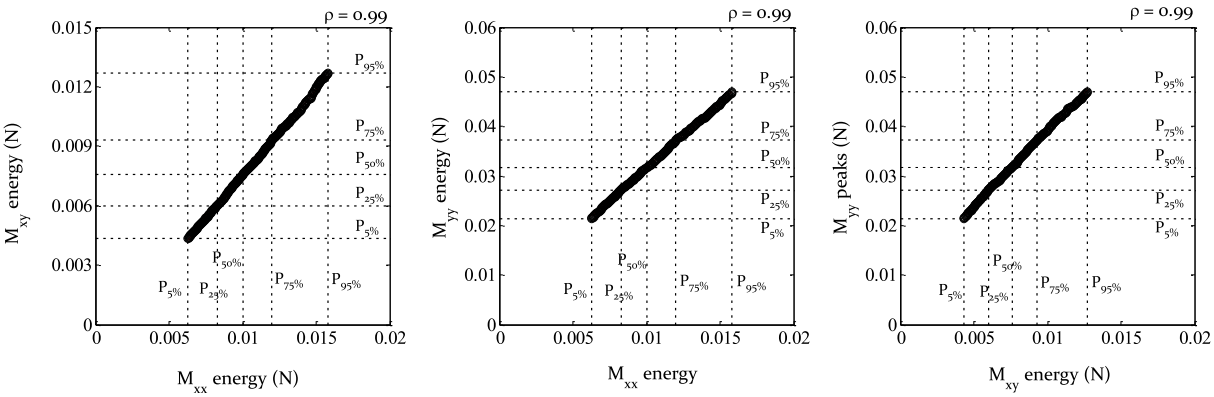

(b) q–q plots considering the elastic strain energy

Fig. 10. Correlation assessment from $N_{simul} = 2000$ simulations (truncation within 95% confidence levels).

(Fig. 11) – model P5%, model P25%, model P50%, model P75% and model P95% –, a total of 266 dynamic analyses were performed. In practice, the response includes a total of 2000 samples with different material and geometrical inputs, for which a confidence level of 95% is assured by the lower (model P5%) and upper (model P95%) limits. Continuous IDA curves were found for each macro-model by assuming a linear interpolation between the discrete result pairs (IM, δ_{EDP}) (Fig. 13).

From Fig. 13, one can conclude on the sudden increase of the out-of-plane displacement after a PGA of $0.4g$, $0.5g$, and $0.6g$ for the models that represent the percentile 5%, percentile 25% and median of the homogenized material curves, respectively. A clear development of a degrading plateau is observed after. In converse, the remaining two models (P75% and P95%) have higher strength values and the difference on the displacements found is significantly lower. In these models, the onset of degrading effects is visible for IM higher than $0.7g$. Furthermore, the conditional dispersion of results in terms of IM and EDP is higher for the P5% model. Such finding is somehow expected since the latter input is associated with low strength values, hence more sensitive to the variability of ground motion characteristics. For the P50% model, it is noticeable that the inelastic phase is well-marked for PGA higher than $0.7g$. Although with different seismic loading input, the latter is consistent with the experimental observations, as no visible damage was obtained until a PGA of $0.56g$ [105].At last, the reader is advised that the interpretation of any structural resurrection in the IDA curves of Fig. 13 is merely an effect of the plot since it does not occur.

Before delving in the damage analysis, two remarks are important to be addressed: (i) the computational advantage of the two-step procedure, and (ii) the computational advantage of the assumption to propagate uncertainty through a reduced number of representative homogenized constitutive curves (Section 4.2.1). Regarding the first, a mesh size of 200 mm was defined for the structural analysis since it provides good estimations when compared to finer meshes [76]. The associated processing time cost per analysis is dependent on the level of damage (non-linearities) but range around 15–25 min. This is a great achievement especially if one notices that each analysis may require 10× more time with a continuous FE macro-modelling strategy based on a 'total strain crack model' and with the same mesh size [76]. A laptop with an i7-4710MQ CPU, 16 GB of RAM (DDR2), and an SSD disk with a writing velocity of 512 Mbytes/s was used to conduct such comparison. Note that total strain crack models are, in the realm of FE continuum analysis, the most convenient for the analysis of larger-scale structures. The difference between estimated processing times is well marked in Fig. 14. Regarding the second point, it is rather clear how the proposed strategy of propagating the material and geometric uncertainty through a reduced yet representative number of homogenized constitutive laws brings a huge reduction in the computation time. Considering the IDA curves of Fig. 15, a total processing time of ≈ 3.6 days is required. Instead, it would be rather impractical to run the whole probabilistic sample of 2000 curves even with the two-step discrete numerical model.

4.4. Damage analysis

4.4.1. Performance levels of the structure

Damage analysis through seismic fragility curves are paramount for decision making and are part of current state-of-art performance-based earthquake engineering (PBEE) frameworks [12]. Fragility curves give the conditional distribution of the probability of exceeding a specific performance state limit (or demand parameter) as a function of an

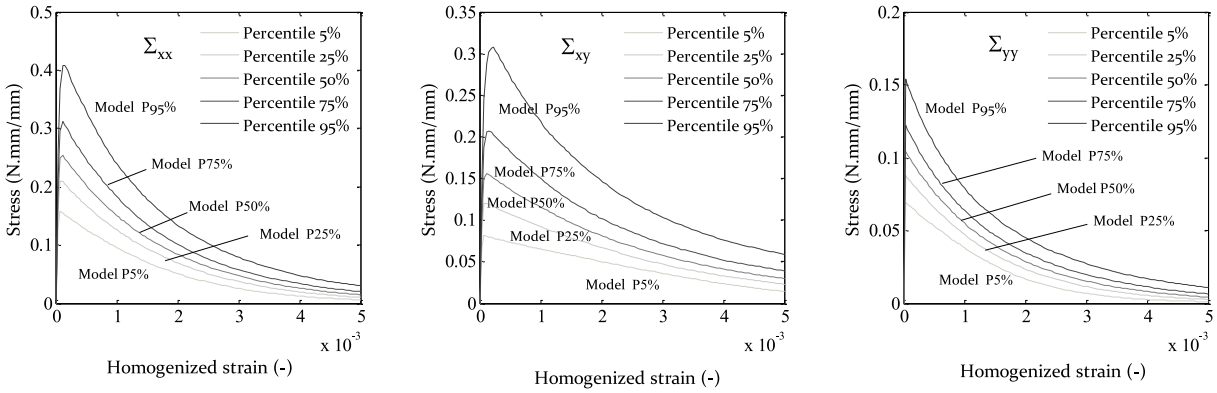

(a) in−plane Σ−E curves

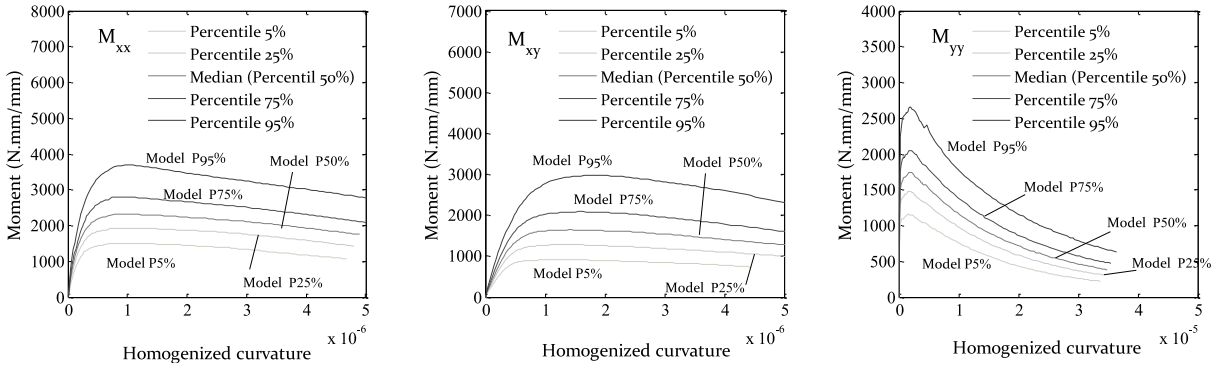

(b) out−of−plane M−χ curves

Fig. 11. Definition of the five input models that represent the total simulated $N_{simul} = 2000$ samples.

IM of the hazard. Defining realistic performance states expressed by discrete thresholds for the EDP on the structure's response is the main struggle of the process.

The selection of a displacement-based parameters as EDP (usually drift values) tends to be generally used by guidelines [48,49,108–112] and in literature-related works [104,105,113]. Again, this supports the decision over a displacement quantity to serve as EDP. A comprehensive overview of the seismic performance code provisions in terms of drift-ratio values is addressed in [114]. Guidelines are especially suitable for in-plane failure modes and a better insight into the safety margin due to out-of-plane collapses is still needed [115]. Moreover, most of the existing URM buildings generally lack a box-type behaviour and the response may be conditioned by the fragility of local structural components. In this scope, such traditional URM structures feature a seismic fragility that is hardly consistent with the provisions given by standards [48,49,115].

For the present study, three damage levels were defined according to Eurocode 8 [49]: damage limitation (DL), significant (or severe) damage (SD) and near collapse (NC). The performance limit states are attained from the results of non-linear static analyses conducted (mesh size of 200 mm) with the model with median material parameters (model P50%), as depicted in Fig. 15 and expressed in Table 3. Note that:

- The DL region implies that the building is safe to be occupied after the earthquake. The limit state is described as δ_{DL} and given by the yielding point of the capacity curve.
- The SD region implies that the building shows clear damage, but still retains a seismic safety margin. The limit state is described as δ_{SD} and it is equal to $0.75\delta_{NC}$ as denoted in Eurocode 8 [49] (δ_{NC} is the NC limit state).
- The NC region implies that the building is severally damaged and, even though it still stands under gravity loads, it has no seismic safety margin. The limit state is described as δ_{NC} and given as the post-peak displacement for which the structure loses 20% of the peak strength capacity (according to [105]).

Table 3
Structural performance levels adopted (longitudinal direction only).

Limit state (LS)	Negative direction (−Y)		Positive direction (+Y)	
	δ_{EDP} (mm)	CoV (%)	δ_{EDP} (mm)	CoV (%)
DL	−0.66	15%	0.45	15%
SD	−3.94	15%	2.65	15%
NC	−5.24	15%	3.53	15%

The different performance limits are presented in Table 3 for each longitudinal direction of the structure because the structure is not symmetric. In this regard, a weakest link approach is considered, meaning that the overall damage state of the structure is given by the limit value that is firstly exceeded according to the displacement δ_{EDP} sign.

4.4.2. Displacement-based seismic fragility curves

The generation of seismic fragility curves constitutes the last step of the framework. According to the defined performance limit states, and with the structural response information for a series of ground motions, such fragility expressions can be expressed. To this aim, the optimization problem given in Eq. (9) is solved through the so-called maximum likelihood method [91]. The estimated log-normal distribution parameters $\hat{\theta}$ and $\hat{\beta}$ were computed for each limit state, see Table 4. Median values $\hat{\theta}$ of the fragility curves are between $0.15g$–$0.29g$, $0.37g$–$0.73g$ and

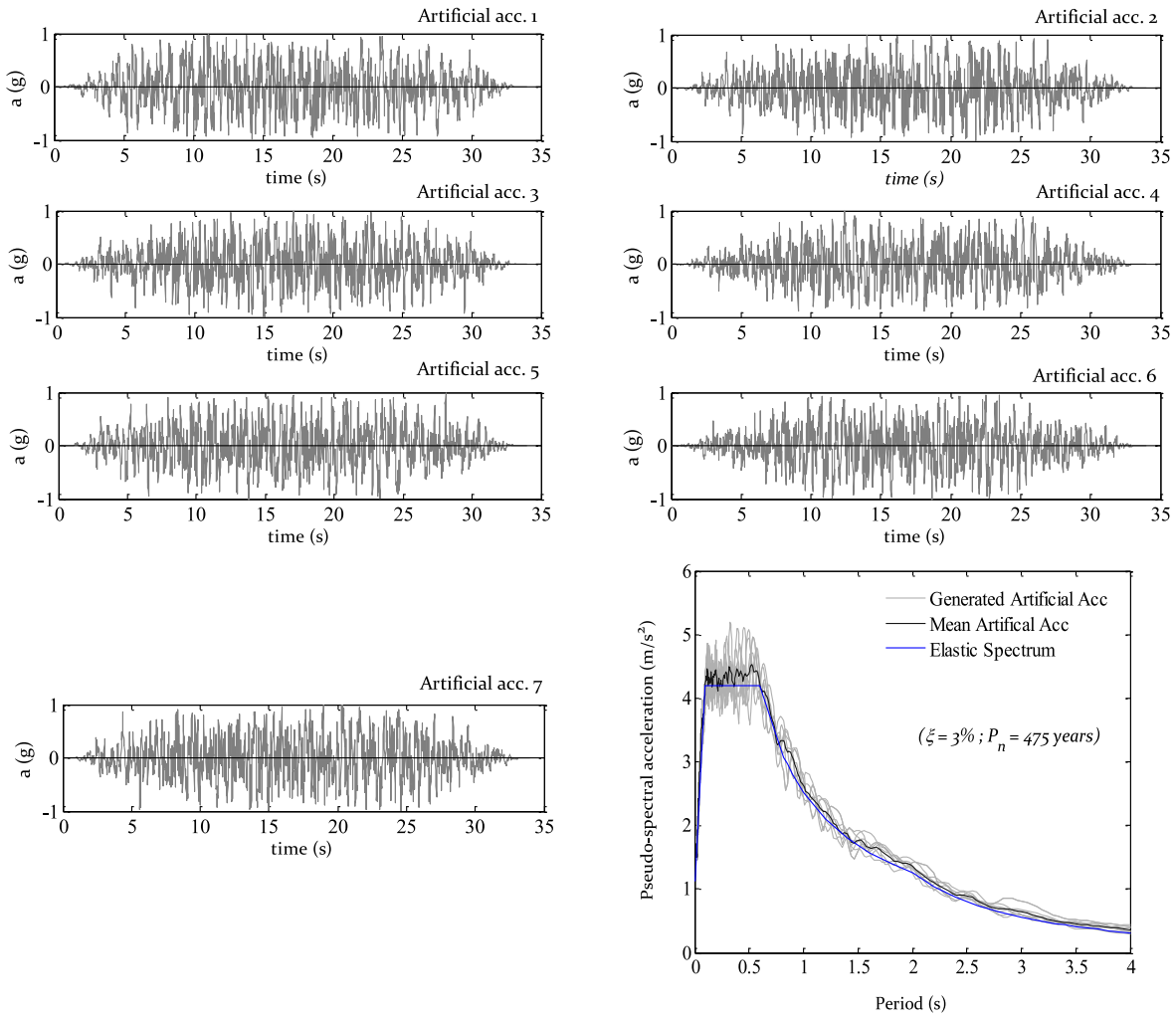

Fig. 12. Artificial generated accelerograms scaled for a peak ground acceleration of 1 m/s^2 and corresponding pseudo-acceleration response-spectrum superposed with the elastic spectrum from Eurocode 8 [49] elastic spectrum.

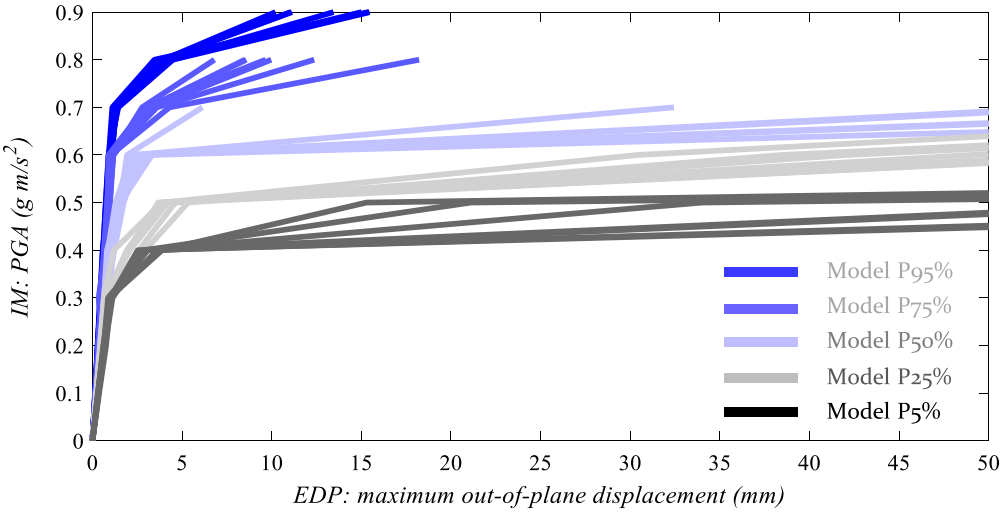

Fig. 13. IDA curves obtained for each of the five defined macro-models.

0.44g–0.84g for the DL, SD and NC states, respectively. The relative difference between the median $\hat{\theta}$ for P95% and P5% results is, for all the damage states, approximated and in the range of 200%. This is a relevant value and may be explained by the considerable variability of the macro-input, which propagates from the material and mechanical uncertainties of the system.

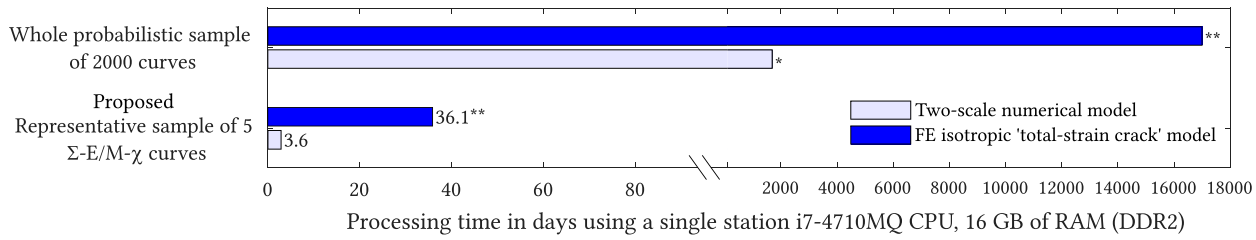

* Estimated considering that each dynamic analysis requires 25min of processing time

** Estimated considering that each dynamic analysis requires 10x more than the two-scale model (as observed in [76])

Fig. 14. Estimated processing times for the simulation of a full probabilistic sample of 2000 curves or using the proposed approach of using only 5 representative curves: processing time between the used two-scale numerical model and a continuum FE 'total-strain crack' model.

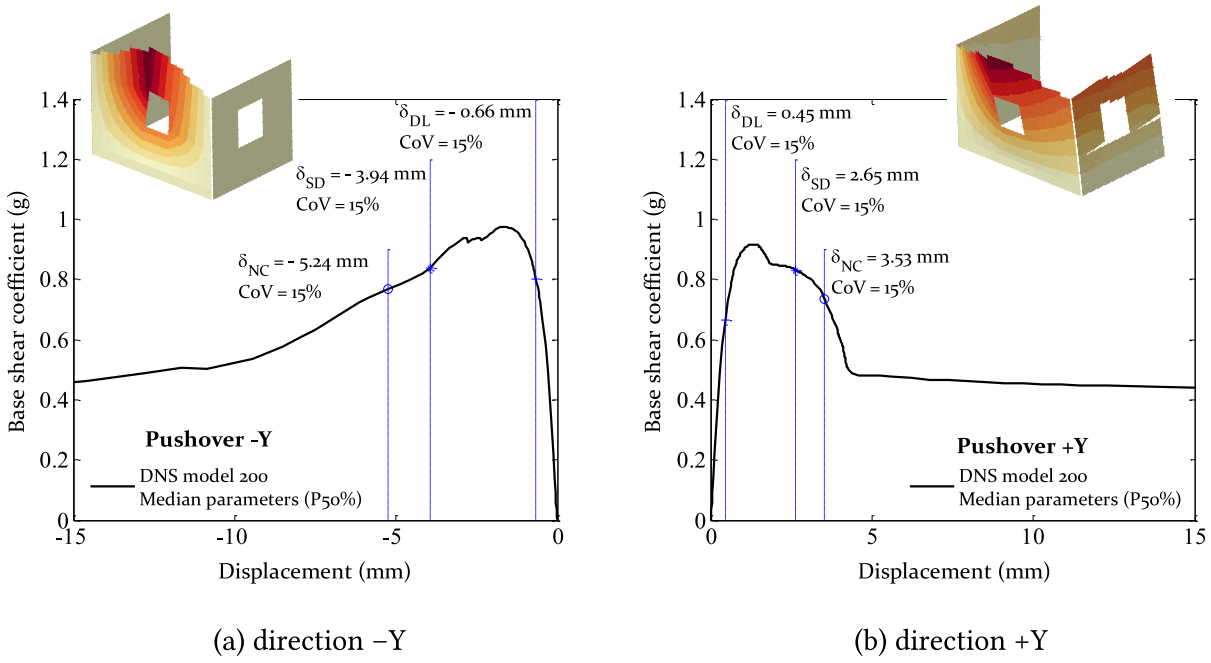

Fig. 15. Obtained non-linear pushover curves with indication of the assumed performance limit states (LS).

Fig. 16 presents the seismic fragility curves found for each damage state. Results allow concluding with a 100% probability and within a 95% confidence level that: (i) the structure will yield for a PGA equal or higher than $\approx 0.45g$; the structure will suffer significant damage for a PGA equal or higher than $\approx 0.85g$; and that the structure will collapse for a PGA equal or higher than $\approx 0.95g$. Such results are close to experimental evidence, as although different loading input was used, the structures witnessed a residual damage for a PGA of $0.56g$, moderate damage for a PGA of $0.84g$, and the collapse for a PGA of $1.27g$.

One may also remark the low capacity of the structure to withstand damage, as the structure can go from a situation of relevant damage to collapse with a PGA increment of only $0.1g$. Note that the performance targets δ_{SD} and δ_{NC} (Fig. 15) are close to each other and a low ductility index exists, which allow understanding the fragile character of the masonry structure demonstrated by the steep shape of the fragility curves of Fig. 16. Additionally to the associated OOP fragility of the structure, the results from the damage assessment may be conservative because the LS are found through a static analysis.

It is also noteworthy to recall that the use of artificial accelerograms, together with the use of the minimum number of motions required by the Eurocode 8 [49], led to a low record-to-record variability. Such low record variability justifies the assumption of presenting the fragility curves of Fig. 16 following a 'deterministic' fashion. A more distributed damage probability could be achieved for the mean curve if the P5%, P25%, P50%, P75%, P95% are combined assuming different weights, for instance a higher contribution for the lower limits aiming to be conservative. However, as the decision is dependent upon the specific results and lacks a general applicability, it was not pursued here..

In this regard and for the case study, the definition of strengthening schemes to postpone the out-of-plane failure of the tympanum wall seems fundamental to reduce human and economic losses in the aftermath of a seismic event. Nevertheless, such a decision should be made simultaneously with information from a hazard probability curve (a potential future streamline of this research).

5. Conclusions

A numerical strategy was presented for the probabilistic structural analysis of masonry structures. The strategy was integrated within a framework with background on the existing PBEE approaches [83], albeit considering the structural and damage analyses only (hazard analysis and loss estimation were disregarded). The approach gathers two levels of analysis: (i) at a meso-scale, in which material, mechanical and geometrical variables are parametrized to carry the masonry uncertainty and compute the random homogenized quantities; and (ii) at a macro-scale, in which the meso-scale uncertainty is propagated through

Table 4
Estimated parameters for the log-normal distributions of the fragility curves for five studied macro-models and for each limit state.

Limit states (LS)	Model P5%		Model P25%		Model P50%		Model P75%		Model P95%	
	$\hat{\theta}$	$\hat{\beta}$	$\hat{\theta}$	$\hat{\beta}$	$\hat{\theta}$	$\hat{\beta}$	$\hat{\theta}$	$\hat{\beta}$	$\hat{\theta}$	$\hat{\beta}$
DL	0.15	0.06	0.17	0.28	0.18	0.25	0.25	0.22	0.29	0.16
SD	0.37	0.13	0.43	0.06	0.59	0.06	0.63	0.04	0.73	0.04
NC	0.44	0.02	0.52	0.05	0.64	0.05	0.72	0.03	0.84	0.04

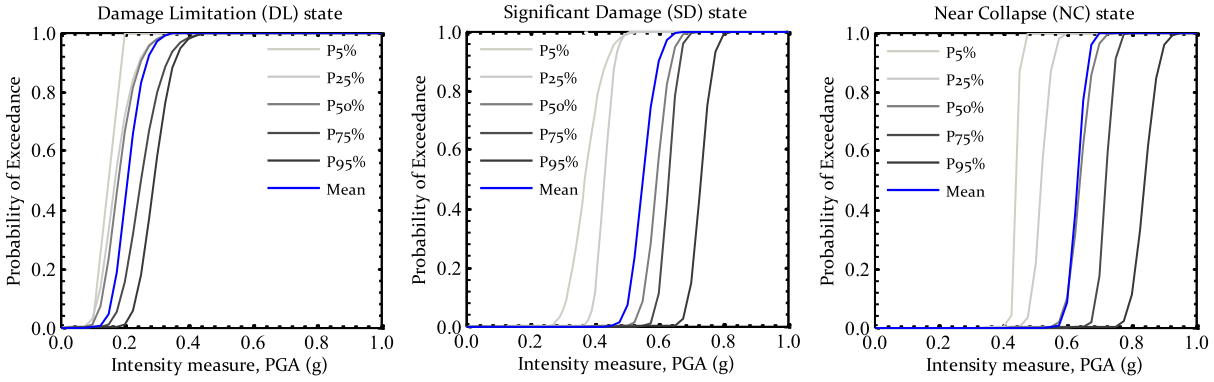

(a) damage limitation (DL) state (b) significant damage (SD) state (c) near collapse (NC) state

Fig. 16. Seismic fragility curves obtained for each of the studied macro-models and for each damage state.

the selection of representative $\Sigma - E$ and $M - \chi$ curves to be used within a discrete-based model. Here, the loading uncertainty is also ensured by using several ground motions compliant with the Eurocode 8 [49] elastic spectrum.

The seismic fragility assessment of a masonry structure was developed to attest the adequacy of the framework. The case study is an English-bond brick house mock-up tested in LNEC by Candeias et al. [93]. Analytical fragility functions were derived from incremental dynamic analysis (IDA), in which a successive set of ground motions (a total of seven) scaled for different PGA levels (intensity measure) were applied to the structure. The response of the structure was evaluated according to an engineering demand parameter (EDP) given by the out-of-plane displacement component of the top gable wall node. A total of 2000 homogenized curves were collected at a meso-scale, whose sample served to perform 266 dynamic analyses at a macro-scale. Such extensive numerical data allowed to compute three displacement-based log-normal fragility functions for the three damage states in which a 95% confidence level was acquired. A maximum-likelihood method was used to estimate the fitted log-normal distribution parameters for three damage limit states that follow Eurocode 8 [49] recommendations, i.e. damage limitation, significant damage and near collapse states. The corresponding limit states (LS) were defined from ad-hoc quasi-static pushover curves obtained from a model with median properties. Main remarks are: (i) the fragility curves that define the 95% confidence level envelope show, for all the damage states considered, a well distinct response. This highlights the relative effect that the system uncertainties have in the response; (ii) the observation supports the experimental campaign, as there are 100% of probability that the structure will suffer significant damage for a PGA higher than $0.85g$; and that the structure will collapse for a PGA equal or higher than $0.95g$; (iii) the structure shows low capacity to dissipate energy, as low standard deviation values were identified for the significant and near collapse damage states.

The case study is suitable to demonstrate that the framework is applicable and computationally attractive when compared to existing advanced numerical strategies for the non-linear dynamic study of masonry. Additionally, the model is based on an analytical methodology with further space for improvement and research, namely: (i) the study of the ideal number of simulations required at a meso-scale; (ii) the study on the effect of performance limit states; (iii) the study on the relative effect of the loading uncertainty when compared with the material one; (iv) the adoption of other IM apart from the structure-independent PGA measure; (v) the use of a methodology within a broader application, perhaps in larger and complex structures; (vi) the integration within other frameworks for reliability assessment [116], and (vii) the integration of the probabilistic model within other types of analysis, such as hazard and loss analyses.

Declaration of competing interest

The authors declare that they have no known competing financial interests or personal relationships that could have appeared to influence the work reported in this paper.

References

[1] Freddi F, Galasso C, Cremen G, Dall'Asta A, Di Sarno L, Giaralis A, et al. Innovations in earthquake risk reduction for resilience: Recent advances and challenges. Int J Disaster Risk Reduct 2021;60:102267. http://dx.doi.org/10.1016/j.ijdrr.2021.102267, URL https://www.sciencedirect.com/science/article/pii/S2212420921002338.

[2] United Nations. Sendai framework for disaster risk reduction 2015–2030. Tech. Rep., Geneve, Switzerland: United Nations Office for Risk Reduction; 2015, p. 32, URL https://www.preventionweb.net/files/43291_sendaiframeworkfordrren.pdf.

[3] de Felice G, De Santis S, Lourenço PB, Mendes N. Methods and challenges for the seismic assessment of historic masonry structures. Int J Archit Herit 2017;11(1):143–60. http://dx.doi.org/10.1080/15583058.2016.1238976.

[4] Funari MF, Silva LC, Mousavian E, Lourenço PB. Real-time structural stability of domes through limit analysis: Application to St. Peter's dome. Int J Archit Herit 2021;1–23. http://dx.doi.org/10.1080/15583058.2021.1992539.

[5] Funari MF, Silva LC, Savalle N, Lourenço PB. A concurrent micro/macro FE-model optimized with a limit analysis tool for the assessment of dry-joint masonry structures. Int J Multiscale Comput Eng 2022;20(5):65–85. http://dx.doi.org/10.1615/IntJMultCompEng.2021040212.

[6] Dauda JA, Silva LC, Lourenço PB, Iuorio O. Out-of-plane loaded masonry walls retrofitted with oriented strand boards: Numerical analysis and influencing parameters. Eng Struct 2021;243:112683. http://dx.doi.org/10.1016/j.engstruct.2021.112683, URL https://www.sciencedirect.com/science/article/pii/S0141029621008336.

[7] Asıkoglu A, Avsar O, Lourenço PB, Silva LC. Effectiveness of seismic retrofitting of a historical masonry structure: Kütahya Kurşunlu Mosque, Turkey. Bull Earthq Eng 2019;17(6):3365–95. http://dx.doi.org/10.1007/s10518-019-00603-6.

[8] Penna A, Morandi P, Rota M, Manzini CF, da Porto F, Magenes G. Performance of masonry buildings during the Emilia 2012 earthquake. Bull Earthq Eng 2014;12(5):2255–73. http://dx.doi.org/10.1007/s10518-013-9496-6.

[9] Vaculik J, Griffith MC. Out-of-plane shaketable testing of unreinforced masonry walls in two-way bending. Bull Earthq Eng 2018. http://dx.doi.org/10.1007/s10518-017-0282-8.

[10] Formisano A, Vaiano G, Fabbrocino F, Milani G. Seismic vulnerability of Italian masonry churches: The case of the Nativity of Blessed Virgin Mary in Stellata of Bondeno. J Build Eng 2018;20:179–200. http://dx.doi.org/10.1016/j.jobe.2018.07.017, URL https://www.sciencedirect.com/science/article/pii/S2352710218306326.

[11] Clementi F, Gazzani V, Poiani M, Lenci S. Assessment of seismic behaviour of heritage masonry buildings using numerical modelling. J Build Eng 2016;8:29–47. http://dx.doi.org/10.1016/j.jobe.2016.09.005, URL https://www.sciencedirect.com/science/article/pii/S2352710216300791.

[12] Günay S, Mosalam KM. PEER performance-based earthquake engineering methodology, revisited. J Earthq Eng 2013;17(6):829–58. http://dx.doi.org/10.1080/13632469.2013.787377.

[13] Leggieri V, Ruggieri S, Zagari G, Uva G. Appraising seismic vulnerability of masonry aggregates through an automated mechanical-typological approach. Autom Constr 2021;132:103972. http://dx.doi.org/10.1016/j.autcon.2021.103972, URL https://www.sciencedirect.com/science/article/pii/S0926580521004234.

[14] Ruggieri S, Tosto C, Rosati G, Uva G, Ferro GA. Seismic vulnerability analysis of masonry churches in piemonte after 2003 valle scrivia earthquake: Post-event screening and situation 17 years later. Int J Archit Herit 2022;16(5):717–45. http://dx.doi.org/10.1080/15583058.2020.1841366.

[15] Rosti A, Del Gaudio C, Rota M, Ricci P, Di Ludovico M, Penna A, et al. Empirical fragility curves for Italian residential RC buildings. Bull Earthq Eng 2021;19(8):3165–83. http://dx.doi.org/10.1007/s10518-020-00971-4.

[16] Uva G, Sanjust CA, Casolo S, Mezzina M. ANTAEUS project for the regional vulnerability assessment of the current building stock in historical centers. Int J Archit Herit 2016;10(1):20–43. http://dx.doi.org/10.1080/15583058.2014.935983.

[17] Ruggieri S, Porco F, Uva G, Vamvatsikos D. Two frugal options to assess class fragility and seismic safety for low-rise reinforced concrete school buildings in Southern Italy. Bull Earthq Eng 2021;19(3):1415–39. http://dx.doi.org/10.1007/s10518-020-01033-5.

[18] Maio R, Vicente R, Formisano A, Varum H. Seismic vulnerability of building aggregates through hybrid and indirect assessment techniques. Bull Earthq Eng 2015;13(10):2995–3014. http://dx.doi.org/10.1007/s10518-015-9747-9.

[19] Chieffo N, Clementi F, Formisano A, Lenci S. Comparative fragility methods for seismic assessment of masonry buildings located in Muccia (Italy). J Build Eng 2019;25:100813. http://dx.doi.org/10.1016/j.jobe.2019.100813, URL https://www.sciencedirect.com/science/article/pii/S2352710219306497.

[20] Ferreira TM, Costa AA, Costa A. Analysis of the out-of-plane seismic behavior of unreinforced masonry: A literature review. Int J Archit Herit 2014;9(8):949–72. http://dx.doi.org/10.1080/15583058.2014.885996.

[21] Ferreira TM, Costa AA, Vicente R, Varum H. A simplified four-branch model for the analytical study of the out-of-plane performance of regular stone URM walls. Eng Struct 2015;83:140–53. http://dx.doi.org/10.1016/j.engstruct.2014.10.048.

[22] D'Altri AM, Sarhosis V, Milani G, Rots J, Cattari S, Lagomarsino S, et al. Modeling strategies for the computational analysis of unreinforced masonry structures: Review and classification. Arch Comput Methods Eng 2019. http://dx.doi.org/10.1007/s11831-019-09351-x.

[23] Lourenço PB, Funari MF, Silva LC. Building resilience and masonry structures : How can computational modelling help? In: Meschke G, Pichler B, Rots JG, editors. Computational modelling of concrete and concrete structures. 1st ed. London: CRC Press; 2022, p. 30–7. http://dx.doi.org/10.1201/9781003316404-4.

[24] Cascini L, Gagliardo R, Portioli F. LiABlock_3D: A software tool for collapse mechanism analysis of historic masonry structures. Int J Archit Herit 2018;1–20. http://dx.doi.org/10.1080/15583058.2018.1509155.

[25] de Felice G, Giannini R. Out-of-plane seismic resistance of masonry walls. J Earthq Eng 2001;5(2):253–71. http://dx.doi.org/10.1080/13632460109350394.

[26] Funari MF, Pulatsu B, Szabó S, Lourenço PB. A solution for the frictional resistance in macro-block limit analysis of non-periodic masonry. Structures 2022;43:847–59. http://dx.doi.org/10.1016/j.istruc.2022.06.072, URL https://www.sciencedirect.com/science/article/pii/S2352012422005525.

[27] D'Ayala D, Speranza E. Definition of collapse mechanisms and seismic vulnerability of historic masonry buildings. Earthq Spectr 2003;19(3):479–509. http://dx.doi.org/10.1193/1.1599896.

[28] Funari MF, Silva LC, Lonetti P, Spadea S, Lourenço PB. Numerical simulation of fracture in layered and sandwich structures: A systematic literature review. Compos Part C: Open Access 2022;100294. http://dx.doi.org/10.1016/j.jcomc.2022.100294, URL https://www.sciencedirect.com/science/article/pii/S2666682022000585.

[29] Baraldi D, Reccia E, Cecchi A. In plane loaded masonry walls: DEM and FEM/DEM models. A critical review. Meccanica 2018;53(7):1613–28. http://dx.doi.org/10.1007/s11012-017-0704-3.

[30] Savalle N, Vincens E, Hans S. Experimental and numerical studies on scaled-down dry-joint retaining walls: Pseudo-static approach to quantify the resistance of a dry-joint brick retaining wall. Bull Earthq Eng 2020;18(2):581–606. http://dx.doi.org/10.1007/s10518-019-00670-9.

[31] Lemos JV. Discrete element modeling of masonry structures. Int J Archit Herit 2007;1(2):190–213. http://dx.doi.org/10.1080/15583050601176868.

[32] Lemos JV. Discrete element modeling of the seismic behavior of masonry construction. Buildings 2019;9(2). http://dx.doi.org/10.3390/buildings9020043.

[33] Bui TT, Limam A, Sarhosis V, Hjiaj M. Discrete element modelling of the in-plane and out-of-plane behaviour of dry-joint masonry wall constructions. Eng Struct 2017;136(October):277–94. http://dx.doi.org/10.1016/j.engstruct.2017.01.020.

[34] Gonen S, Pulatsu B, Erdogmus E, Karaesmen E, Karaesmen E. Quasi-static nonlinear seismic assessment of a fourth century A.D. Roman Aqueduct in Istanbul, Turkey. Heritage 2021;4(1):401–21. http://dx.doi.org/10.3390/heritage4010025.

[35] Otero F, Oller S, Martinez X, Salomón O. Numerical homogenization for composite materials analysis. Comparison with other micro mechanical formulations. Compos Struct 2015;122:405–16. http://dx.doi.org/10.1016/j.compstruct.2014.11.041, URL http://linkinghub.elsevier.com/retrieve/pii/S0263822314006102.

[36] Lourenço PB, Silva LC. Computational applications in masonry structures: from the meso-scale to the super-large/super-complex. Int J Multiscale Comput Eng 2020;18(1):1–30. http://dx.doi.org/10.1615/IntJMultCompEng.2020030889.

[37] Reccia E, Leonetti L, Trovalusci P, Cecchi A. A multiscale/multidomain model for the failure analysis of masonry walls: a validation with a combined FEM/DEM approach. Int J Multiscale Comput Eng 2018;16(4):325–43. http://dx.doi.org/10.1615/IntJMultCompEng.2018026988.

[38] Milani G, Venturini G. Automatic fragility curve evaluation of masonry churches accounting for partial collapses by means of 3D FE homogenized limit analysis. Comput Struct 2011;89(17–18):1628–48. http://dx.doi.org/10.1016/j.compstruc.2011.04.014.

[39] Bertolesi E, Silva LC, Milani G. Validation of a two-step simplified compatible homogenisation approach extended to out-plane loaded masonries. Int J Mason Res Innov 2019;4:265. http://dx.doi.org/10.1504/IJMRI.2019.10019407.

[40] Sharma S, Silva LC, Graziotti F, Magenes G, Milani G. Modelling the experimental seismic out-of-plane two-way bending response of unreinforced periodic masonry panels using a non-linear discrete homogenized strategy. Eng Struct 2021;242(December 2020). http://dx.doi.org/10.1016/j.engstruct.2021.112524.

[41] Casolo S, Milani G. Simplified out-of-plane modelling of three-leaf masonry walls accounting for the material texture. Constr Build Mater 2013;40:330–51. http://dx.doi.org/10.1016/j.conbuildmat.2012.09.090.

[42] Caliò I, Marletta M, Pantò B. A new discrete element model for the evaluation of the seismic behaviour of unreinforced masonry buildings. Eng Struct 2012;40:327–38. http://dx.doi.org/10.1016/j.engstruct.2012.02.039.

[43] Vadalà F, Cusmano V, Funari MF, Caliò I, Lourenço PB. On the use of a mesoscale masonry pattern representation in discrete macro-element approach. J Build Eng 2022;50:104182. http://dx.doi.org/10.1016/j.jobe.2022.104182.

[44] Cannizzaro F, Pantò B, Caddemi S, Caliò I. A Discrete Macro-Element Method (DMEM) for the nonlinear structural assessment of masonry arches. Eng Struct 2018;168(October 2020):243–56. http://dx.doi.org/10.1016/j.engstruct.2018.04.006.

[45] Tomić I, Vanin F, Beyer K. Uncertainties in the seismic assessment of historical masonry buildings. 2021, http://dx.doi.org/10.3390/app11052280.

[46] Benedetti A, Tarozzi M. Interpretation formulas for in situ characterization of mortar strength. Constr Build Mater 2020;242:118093. http://dx.doi.org/10.1016/j.conbuildmat.2020.118093, URL https://www.sciencedirect.com/science/article/pii/S0950061820300982.

[47] Martakis P, Reuland Y, Imesch M, Chatzi E. Reducing uncertainty in seismic assessment of multiple masonry buildings based on monitored demolitions. Bull Earthq Eng 2022. http://dx.doi.org/10.1007/s10518-022-01369-0.

[48] ASCE/SEI41-17. Seismic evaluation and retrofit of existing buildings. ASCE/SEI, 4th ed. American Society of Civil Engineers; 2017, http://dx.doi.org/10.1061/9780784408841.

[49] CEN. Eurocode 8: Design of structures for earthquake resistance. Part 1: General rules, seismic actions and rules for buildings. Eurocode en 1998-1. European Committee for Standardization (CEN), Brussels; 2004.

[50] Norio O, Ye T, Kajitani Y, Shi P, Tatano H. The 2011 eastern Japan great earthquake disaster: Overview and comments. Int J Disaster Risk Sci 2011;2(1):34–42. http://dx.doi.org/10.1007/s13753-011-0004-9.

[51] Iervolino I. Assessing uncertainty in estimation of seismic response for PBEE. Earthq Eng Struct Dyn 2017;46(10):1711–23. http://dx.doi.org/10.1002/eqe.2883.

[52] Ghosh S, Ghosh S, Chakraborty S. Seismic fragility analysis in the probabilistic performance-based earthquake engineering framework: an overview. Int J Adv Eng Sci Appl Math 2021;13(1):122–35. http://dx.doi.org/10.1007/s12572-017-0200-y.

[53] Shittu AA, Kolios A, Mehmanparast A. A systematic review of structural reliability methods for deformation and fatigue analysis of offshore jacket structures. In: Metals. vol. 11, (1). 2021, http://dx.doi.org/10.3390/met11010050.

[54] Bartoli G, Betti M, Marra AM, Monchetti S. A Bayesian model updating framework for robust seismic fragility analysis of non-isolated historic masonry towers. Phil Trans R Soc A 2019;377(2155):20190024. http://dx.doi.org/10.1098/rsta.2019.0024.

[55] Grant DN, Dennis J, Sturt R, Milan G, McLennan D, Negrette P, et al. Explicit modelling of collapse for Dutch unreinforced masonry building typology fragility functions. Bull Earthq Eng 2021;19(15):6497–519. http://dx.doi.org/10.1007/s10518-020-00923-y.

[56] Park J, Towashiraporn P, Craig JI, Goodno BJ. Seismic fragility analysis of low-rise unreinforced masonry structures. Eng Struct 2009;31(1):125–37. http://dx.doi.org/10.1016/j.engstruct.2008.07.021.

[57] Chácara C, Cannizzaro F, Pantò B, Caliò I, Lourenço PB. Seismic vulnerability of URM structures based on a Discrete Macro-Element Modeling (DMEM) approach. Eng Struct 2019;201:109715. http://dx.doi.org/10.1016/j.engstruct.2019.109715, URL https://www.sciencedirect.com/science/article/pii/S0141029619304948.

[58] Gonen S, Pulatsu B, Soyoz S, Erdogmus E. Stochastic discontinuum analysis of unreinforced masonry walls: Lateral capacity and performance assessments. Eng Struct 2021;238:112175. http://dx.doi.org/10.1016/j.engstruct.2021.112175, URL https://www.sciencedirect.com/science/article/pii/S0141029621003254.

[59] Malomo D, DeJong MJ. A Macro-Distinct Element Model (M-DEM) for out-of-plane analysis of unreinforced masonry structures. Eng Struct 2021;244:112754. http://dx.doi.org/10.1016/j.engstruct.2021.112754, URL https://www.sciencedirect.com/science/article/pii/S0141029621009044.

[60] Funari MF, Mehrotra A, Lourenço PB. A tool for the rapid seismic assessment of historic masonry structures based on limit analysis optimisation and rocking dynamics. Appl Sci (Switzerland) 2021;11(3):1–22. http://dx.doi.org/10.3390/app11030942.

[61] Angiolilli M, Lagomarsino S, Cattari S, Degli Abbati S. Seismic fragility assessment of existing masonry buildings in aggregate. Eng Struct 2021;247:113218. http://dx.doi.org/10.1016/j.engstruct.2021.113218, URL https://www.sciencedirect.com/science/article/pii/S0141029621013432.

[62] JCSS. Joint commitee on structural safety - probablistic model code PART 3: Resistance models. Tech. Rep., Technical University of Denmark; 2011, URL http://www.jcss.byg.dtu.dk/Publications/Probabilistic_Model_Code.

[63] Milani G, Lourenço P, Tralli A. Homogenization approach for the limit analysis of out-of-plane loaded masonry walls. J Struct Eng 2006;132(10):1650–63. http://dx.doi.org/10.1061/(ASCE)0733-9445(2006)132:10(1650).

[64] Cecchi A, Sab K. Out of plane model for heterogeneous periodic materials: the case of masonry. Eur J Mech A Solids 2002;21(5):715–46. http://dx.doi.org/10.1016/S0997-7538(02)01243-3.

[65] Trovalusci P, Ostoja-Starzewski M, De Bellis ML, Murrali A. Scale-dependent homogenization of random composites as micropolar continua. Eur J Mech A Solids 2015;49:396–407. http://dx.doi.org/10.1016/j.euromechsol.2014.08.010.

[66] Addessi D, Di Re P, Gatta C, Sacco E. Multiscale analysis of out-of-plane masonry elements using different structural models at macro and microscale. Comput Struct 2021;247:106477. http://dx.doi.org/10.1016/j.compstruc.2020.106477, URL https://www.sciencedirect.com/science/article/pii/S0045794920302807.

[67] Šejnoha M, Janda T, Vorel J, Kucíková L, Padevět P. Combining homogenization, indentation and Bayesian inference in estimating the microfibril angle of spruce. Procedia Eng 2017;190:310–7. http://dx.doi.org/10.1016/j.proeng.2017.05.343, URL http://www.sciencedirect.com/science/article/pii/S1877705817324839.

[68] Silva LC, Lourenço PB, Milani G. Derivation of the out-of-plane behaviour of masonry through homogenization strategies: micro-scale level. Comput Struct 2018;209:30–43. http://dx.doi.org/10.1016/j.compstruc.2018.08.013.

[69] Lourenço PB, Rots JG. Multisurface interface model for analysis of masonry structures. J Eng Mech 1997;123(7):660–8. http://dx.doi.org/10.1061/(ASCE)0733-9399(1997)123:7(660).

[70] Van Zijl G. Computational modelling of masonry creep and shrinkage [Ph.D. thesis; Ph.D. dissertation], Delft University of Technology; 2000, [in English].

[71] Metropolis N, Ulam S. The Monte Carlo Method. J Amer Statist Assoc 1949;44(247):335–41. http://dx.doi.org/10.1080/01621459.1949.10483310.

[72] Stein M. Large sample properties of simulations using latin hypercube sampling. Technometrics 1987;29(2):143–51. http://dx.doi.org/10.1080/00401706.1987.10488205.

[73] McKay MD, Beckman RJ, Conover WJ. Comparison of three methods for selecting values of input variables in the analysis of output from a computer code. Technometrics 1979;21(2):239–45. http://dx.doi.org/10.1080/00401706.1979.10489755.

[74] Abaqus V. 6.14 Documentation. vol. 651, (6.2). Dassault Systemes Simulia Corporation; 2014.

[75] da Silva LCM, Milani G. A FE-Based Macro-Element for the Assessment of Masonry Structures: Linear Static, Vibration, and Non-Linear Cyclic Analyses. In: Applied sciences. 12, (3). 2022, http://dx.doi.org/10.3390/app12031248.

[76] Silva LC, Lourenço PB, Milani G. Numerical homogenization-based seismic assessment of an English-bond masonry prototype: Structural level application. Earthq Eng Struct Dyn 2020;49(9):841–62. http://dx.doi.org/10.1002/eqe.3267.

[77] Faber M, Maes M, Baker J, Vrouwnvelder T, Takada T. Principles of risk assessment of engineered systems. In: Kanda, Takada, Furuta, editors. 10th international conference on applications of statistics and probability in civil engineering. The University of Tokyo, Kashiwa Campus, Japan: Taylor & Francis Group, London; 2007.

[78] Faber M, Stewart M. Risk assessment for civil engineering facilities: critical overview and discussion. Reliab Eng Syst Saf 2003;80(2):173–84. http://dx.doi.org/10.1016/S0951-8320(03)00027-9.

[79] Stewart MG, Melchers RE. Probablistic risk assessment of engineering systems. Springer, ITP; 1997.

[80] Melchers RE, Beck AT. Structural reliability analysis and prediction. John Wiley & Sons Ltd; 2018, http://dx.doi.org/10.1002/9781119266105.

[81] Silva LC. Dynamic analysis of out-of-plane loaded masonry walls using homogenization (Doctoral thesis; Ph.D. thesis), University of Minho, Department of Civil Engineering, Guimarães, Portugal; 2019, p. 191.

[82] Metropolis N, Ulam S. The Monte Carlo Method. J Amer Statist Assoc 1949;44(247):335–41. http://dx.doi.org/10.1080/01621459.1949.10483310, URL https://www.tandfonline.com/doi/abs/10.1080/01621459.1949.10483310.

[83] Krawinkler H, Miranda E. Performance-based earthquake engineering. In: Bozorgnia Y, Bertero VV, editors. Earthquake engineering: from engineering seismology to performance-based engineering. Boca Raton, Florida: CRC Press; 2004, p. 560–636.

[84] Kita A, Cavalagli N, Masciotta MG, Lourenço PB, Ubertini F. Rapid post-earthquake damage localization and quantification in masonry structures through multidimensional non-linear seismic IDA. Eng Struct 2020;219:110841. http://dx.doi.org/10.1016/j.engstruct.2020.110841, URL https://www.sciencedirect.com/science/article/pii/S0141029619351788.

[85] Vamvatsikos D, Cornell CA. Applied incremental dynamic analysis. Earthq Spectr 2004;20(2):523–53. http://dx.doi.org/10.1193/1.1737737.

[86] Vamvatsikos D, Fragiadakis M. Incremental dynamic analysis for estimating seismic performance sensitivity and uncertainty. Int J Earthq Eng Struct Dyn 2010;39(2):141–63. http://dx.doi.org/10.1002/eqe.935.

[87] Pitilakis K, Crowley H, Kaynia AM. SYNER-g: Typology definition and fragility functions for physical elements at seismic risk: Buildings, lifelines, transportation networks and critical facilities. Geotech Geol Earthq Eng 2014;27:1–28. http://dx.doi.org/10.1007/978-94-007-7872-6.

[88] Luco N, Cornell CA. Structure-specific scalar intensity measures for near-source and ordinary earthquake ground motions. Earthq Spectr 2007;23(2):357–92. http://dx.doi.org/10.1193/1.2723158.

[89] Tothong P, Luco N. Probabilistic seismic demand analysis using advanced ground motion intensity measures. Earthq Eng Struct Dyn 2007;36(13):1837–60. http://dx.doi.org/10.1002/eqe.696.

[90] Porter K, Kennedy R, Bachman R. Creating fragility functions for performance-based earthquake engineering. Earthq Spectr 2007;23(2):471–89. http://dx.doi.org/10.1193/1.2720892.

[91] Baker JW. Efficient analytical fragility function fitting using dynamic structural analysis. Earthq Spectr 2014;31(1):579–99. http://dx.doi.org/10.1193/021113EQS025M.

[92] Bakalis K, Vamvatsikos D. Seismic fragility functions via nonlinear response history analysis. J Struct Eng 2018;144(10):04018181. http://dx.doi.org/10.1061/(ASCE)ST.1943-541X.0002141.

[93] Candeias P, Costa AC, Mendes N, Costa A, Lourenço P. Experimental assessment of the out-of-plane performance of masonry buildings through shaking table tests. Int J Archit Herit 2017;11(1).

[94] Mojsilović N, Stewart MG. Probability and structural reliability assessment of mortar joint thickness in load-bearing masonry walls. Struct Saf 2015;52:209–18. http://dx.doi.org/10.1016/j.strusafe.2014.02.005, URL https://www.sciencedirect.com/science/article/pii/S0167473014000186. Engineering Analyses with Vague and Imprecise Information.

[95] Willis C, Griffith M, Lawrence S. Horizontal bending of unreinforced clay brick masonry. Masonry Int 2004;17(3):109–21.

[96] Borri A, Corradi M, Castori G, De Maria A. A method for the analysis and classification of historic masonry. Bull Earthq Eng 2015;13(9):2647–65. http://dx.doi.org/10.1007/s10518-015-9731-4.

[97] Jafari S, Rots JG, Esposito R. Core testing method to assess nonlinear behavior of brick masonry under compression: A comparative experimental study. Constr Build Mater 2019;218:193–205. http://dx.doi.org/10.1016/j.conbuildmat.2019.04.188.

[98] Gelfi P. SIMQKE-GR - Software for generating artificial accelerograms compatible with the response spectrum. 2006.

[99] Silva W, Lee K. WES RASCAL code for synthesizing earthquake ground motions.. Tech. Rep., Washington, DC: Department of the Army, US Army Crops of Engineers; 1987, URL http://www.pacificengineering.org/RascalCode/RASCALCODE.pdf.

[100] Gasparini D, Vanmarke E. Simulated earthquake motions compatible with precribed response spectra. Evaluation of Seismic Safety of Buildings. Tech. Rep., Department of Civil Engineering, Massachusetts Institute of Technology, U.S.A.; 1976.

[101] Vamvatsikos D, Cornell CA. Incremental dynamic analysis. Earthq Eng Struct Dyn 2002;31(3):491–514. http://dx.doi.org/10.1002/eqe.141.

[102] Jalayer F, Cornell CA. Alternative non-linear demand estimation methods for probability-based seismic assessments. Earthq Eng Struct Dyn 2009;38(8):951–72. http://dx.doi.org/10.1002/eqe.876.

[103] Baker JW. Measuring bias in structural response caused by ground motion scaling. In: 8th pacific conference on earthquake engineering, Singapore. vol. 8, 2007.

[104] Calvi G, Pinho R, Magenes G, Bommer J, Restrepo-Vélez L, Crowley H. Development of seismic vulnerability assessment methodologies over the past 30 years. ISET J Eathq Technol 2006;43(3):75–104.

[105] Rota M, Penna A, Magenes G. A methodology for deriving analytical fragility curves for masonry buildings based on stochastic nonlinear analyses. Eng Struct 2010;32(5):1312–23. http://dx.doi.org/10.1016/j.engstruct.2010.01.009.

[106] Frankie TM, Gencturk B, Elnashai AS. Simulation-based fragility relationships for unreinforced masonry buildings. J Struct Eng 2013;139(3):400–10. http://dx.doi.org/10.1061/(ASCE)ST.1943-541X.0000648.

[107] Council BSS. NEHRP recommended provisions for seismic regulations for new buildings and other structures, part 1 provisions. FEMA302, Federal Emergency Management Agency; 1997.

[108] SEAOC. Vision 2000, Performance based seismic engineering of buildings - vol I and II: Conceptual framework. 1995.

[109] Applied Technology Council. Seismic evaluation and retrofit of concrete buildings. 2. Appendices. Tech. Rep., Redwood city; 1996.

[110] FEMA 356. Prestandard and commentary for the seismic rehabiliation of buildings. Tech. Rep., Washington, DC, USA: Federal Emergency Management Agency; 2000.

[111] FEMA. HAZUS 1999. Earthquake loss estimation methodology: technical manual. Washington D.C.: Federal Emergency Management Agency; 1999.

[112] NZSEE. The seismic assessment of existing buildings: Part C8, unreinforced masonry buildings, technical guidelines for engineering assessments. Tech. Rep., Wellington, New Zealand: New Zealand Society for Earthquake Engineering; 2017.

[113] Kappos AJ. An overview of the development of the hybrid method for seismic vulnerability assessment of buildings. Struct Infrastructure Eng 2016;12(12):1573–84. http://dx.doi.org/10.1080/15732479.2016.1151448.

[114] Petry S, Beyer K. Influence of boundary conditions and size effect on the drift capacity of URM walls. Eng Struct 2014;65:76–88. http://dx.doi.org/10.1016/j.engstruct.2014.01.048.

[115] Vanin F, Zaganelli D, Penna A, Beyer K. Estimates for the stiffness, strength and drift capacity of stone masonry walls based on 123 quasi-static cyclic tests reported in the literature. Bull Earthq Eng 2017;15(12):5435–79. http://dx.doi.org/10.1007/s10518-017-0188-5.

[116] Iannacone L, Andreini M, Gardoni P, Sassu M. Probabilistic models and fragility estimates for unreinforced masonry walls subject to in-plane horizontal forces. J Struct Eng 2021;147(6):04021074. http://dx.doi.org/10.1061/(ASCE)ST.1943-541X.0003006.